

Final Report
DESIGN AND DEVELOPMENT OF
A PNEUMATIC GIMBAL ACTUATION SYSTEM

GPO PRICE \$ _____

CFSTI PRICE(S) \$ _____

Hard copy (HC) 3.00Microfiche (MF) 1.65

FACILITY FORM 602

N68-17496

ff 653 July 65

(ACCESSION NUMBER)

(THRU)

(PAGES)

(CODE)

(NASA CR OR TMX OR AD NUMBER)

(CATEGORY)



RESEARCH LABORATORIES DIVISION
SOUTHFIELD, MICHIGAN

Final Report
DESIGN AND DEVELOPMENT OF
A PNEUMATIC GIMBAL ACTUATION SYSTEM

June 1967

Contract NAS 8-5407, Modification No. 10, Phase 1

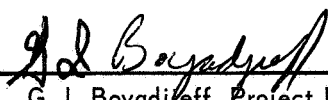
Submitted to

Flight Controls Development Branch
Astrionics Division
NATIONAL AERONAUTICS AND SPACE ADMINISTRATION
Marshall Space Flight Center
Huntsville, Alabama 35812

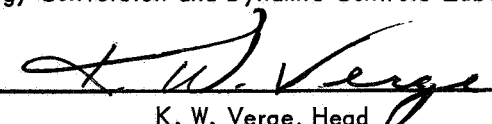
By

Bendix Research Laboratories
Southfield, Michigan 48075

Prepared under
Direction of:


G. I. Boyadjieff, Project Engineer
Flight Controls Department
Energy Conversion and Dynamic Controls Laboratory

Approved by:


K. W. Verge, Head
Flight Controls Department
Energy Conversion and Dynamic Controls Laboratory

Approved by:

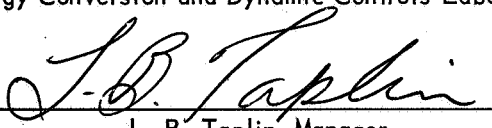

L. B. Taplin, Manager
Energy Conversion and Dynamic Controls Laboratory

TABLE OF CONTENTS

	<u>Page</u>
SECTION 1 - INTRODUCTION AND SUMMARY	1-1
SECTION 2 - SERVOMOTOR DEVELOPMENT	2-1
2.1 Description	2-1
2.1.1 Servomotor Model 3812	2-3
2.1.2 Gear Motor Design	2-3
2.1.2.1 Motor Gears	2-6
2.1.2.2 Bearings	2-6
2.1.2.3 Manifolding	2-6
2.1.2.4 Pressure Balancing	2-9
2.1.2.5 Cross-Porting	2-9
2.1.2.6 Material	2-9
2.2 Analysis	2-12
2.2.1 Performance	2-12
2.2.1.1 Torque-Speed Requirements	2-12
2.2.1.2 Motor Displacement	2-15
2.2.1.3 No Load Speed	2-17
2.2.2 Design	2-19
2.2.2.1 Bearing Loads and Stresses	2-21
2.2.2.2 Gear Tooth Stress Analysis	2-22
2.2.2.3 Pinion Shaft Bending Stress	2-24
2.2.2.4 Output Shaft Torsional Strength	2-25
2.3 Servomotor Tests	2-25
2.3.1 Servomotor Test Setup	2-27
2.3.2 Motor Tests with Nitrogen	2-27
2.3.2.1 Unported Motor	2-27
2.3.2.2 Cross-Porting Area	2-30
2.3.2.3 Ported Motor	2-30
2.3.3 Motor Tests with Hydrogen	2-30
SECTION 3 - SYSTEM EVALUATION	3-1
3.1 Test Fixture	3-1
3.1.1 Load Fixture Instrumentation	3-2
3.1.2 Pneumatic System	3-3
3.1.3 Control System Wiring and Instrumentation	3-3
3.1.4 D.C. Servoamplifier Design	3-3

	<u>Page</u>
3.2 Open-Loop and Closed-Loop Performance	3-7
3.2.1 Rate Compensation	3-7
3.2.2 Pressure Feedback Compensation	3-7
3.3 Conclusions	3-7
APPENDIX A - EFFECT OF THERMAL CYCLING AND CRYOGENIC TEMPERATURES ON ADHESIVE SHEAR STRENGTH	A-1
APPENDIX B - DISPLACEMENT AND OUTPUT TORQUE OF A GEAR MOTOR	B-1

LIST OF ILLUSTRATIONS

<u>Figure No.</u>	<u>Title</u>	<u>Page</u>
1-1	Pneumatic Gear Type Servomotor and Servovalve (Viewed from Servovalve End)	1-2
1-2	J2 Engine Pneumatic Gimbal Actuator	1-2
2-1	Pneumatic Gear Type Servomotor and Servovalve (Viewed from Output Shaft End)	2-2
2-2	Bendix Servovalve Model 3812 Servovalve	2-4
2-3	View of Servovalve Showing Ports	2-4
2-4	Section View of Gear Motor	2-5
2-5	Supply, Load Ports, and Exhaust Manifolds at Servovalve Interface	2-7
2-6	Exhaust Flow Manifolding	2-8
2-7	Pressure Balancing and Exhausting of Leakage Flow Past Sides of Gears	2-10
2-8	Cross-Porting Between Load Port Pressures P_1 and P_2	2-11
2-9	Predicted Servomotor Performance	2-13
2-10	Servomotor Torque-Speed Performance and Requirements	2-26
2-11	Servomotor Test Setup	2-26
2-12	Stall Torque Sensitivity of Unported Servomotor (with Nitrogen)	2-28
2-13	No-Load Speed Sensitivity of Unported Servomotor (with Nitrogen)	2-28
2-14	Performance of Unported Servomotor (with Nitrogen)	2-29
2-15	No-Load Frequency Response of Unported Servomotor (with Nitrogen)	2-29
2-16	Effect of Cross-Port Orifice Area on Servomotor Speed	2-31
2-17	Stall Torque Sensitivity of Ported Servomotor (with Nitrogen)	2-31
2-18	Servomotor Port Pressure at Stall Versus Current (with Nitrogen)	2-32
2-19	Servomotor Port Pressure, Free Running Versus Current (with Nitrogen)	2-32
2-20	Gas Consumption at Stall Versus Current (with Nitrogen)	2-33
2-21	Gas Consumption Free Running, Versus Current (with Nitrogen)	2-33
2-22	Performance of Ported Servomotor (with Nitrogen)	2-34
2-23	No-Load Frequency Response of Ported Servomotor (with Nitrogen)	2-34
2-24	Stall Torque Sensitivity of Ported Servomotor (with Hydrogen)	2-35
2-25	Servomotor Port Pressure at Stall Versus Current (with Hydrogen)	2-35

<u>Figure No.</u>	<u>Title</u>	<u>Page</u>
2-26	Gas Consumption at Stall (with Hydrogen)	2-36
2-27	No-Load Speed Sensitivity of Ported Servomotor (with Hydrogen)	2-36
3-1	Load Fixture and Instrumentation Schematic	3-2
3-2	Pneumatic System Schematic	3-4
3-3	J-2 Instrumentation Diagram	3-5
3-4	J-2 Servoamplifier Block Diagram	3-6
3-5	Pressure Feedback Block Diagram	3-6
3-6	J-2 Actuator Closed Loop Response (Without Friction Load)	3-8
3-7	J-2 Actuator Closed Loop Response (With Friction Load)	3-9
3-8	J-2 Actuator Linearity	3-9
3-9	J-2 Actuator Hysteresis	3-9
3-10	Transient Response Without and With Load Friction	3-10
3-11	Actuator Closed-Loop Frequency Response ($f = 1$ cps to $f = 5$ cps; Actuator Position = 0.060 in.)	3-11
3-12	Actuator Closed-Loop Frequency Response ($f = 6$ cps to $f = 11$ cps; Actuator Position = 0.060 in.)	3-12
3-13	Actuator Closed-Loop Frequency Response ($f = 1$ cps to $f = 6$ cps; Actuator Position = 0.075 in.)	3-13
3-14	Actuator Closed-Loop Frequency Response ($f = 7$ cps to $f = 12$ cps; Actuator Position = 0.075 in.)	3-14
3-15	Frequency Response with Pressure Feedback, No-Load Friction	3-15
3-16	Transient Response with Pressure Feedback	3-16
3-17	Actuator Linearity with Pressure Feedback	3-17
3-18	Actuator Resolution with Pressure Feedback	3-17
A-1	Shear Test Setup	A-2
B-1	Typical Gear Motor Mesh	B-3
B-2	Pressure Profile for Gear	B-3
B-3	Pressure Profile for Pinion	B-5
B-4	Diagram for Determining Output Torque	B-5
B-5	Force Diagram in Motor Gear Mesh	B-7
B-6	Graphical Definition of ϕ , ϕ_m , and λ	B-9

LIST OF TABLES

<u>Table No.</u>	<u>Title</u>	<u>Page</u>
2-1	Servomotor Performance Characteristics	2-1
2-2	Actuator Performance Specifications, Servomotor Requirements and Theoretical Gear Motor Performance	2-13
2-3	Displacement/Area Ratio and Pressure Ratio Comparison	2-16
2-4	Bearing Loads and Stresses for Various Motor Speeds	2-22
A-1	Cryogenic Bond Strength	A-2

14-00000

14-00000

14-00000

14-00000

14-00000

14-00000

14-00000

14-00000

PRECEDING PAGE BLANK NOT FILMED.

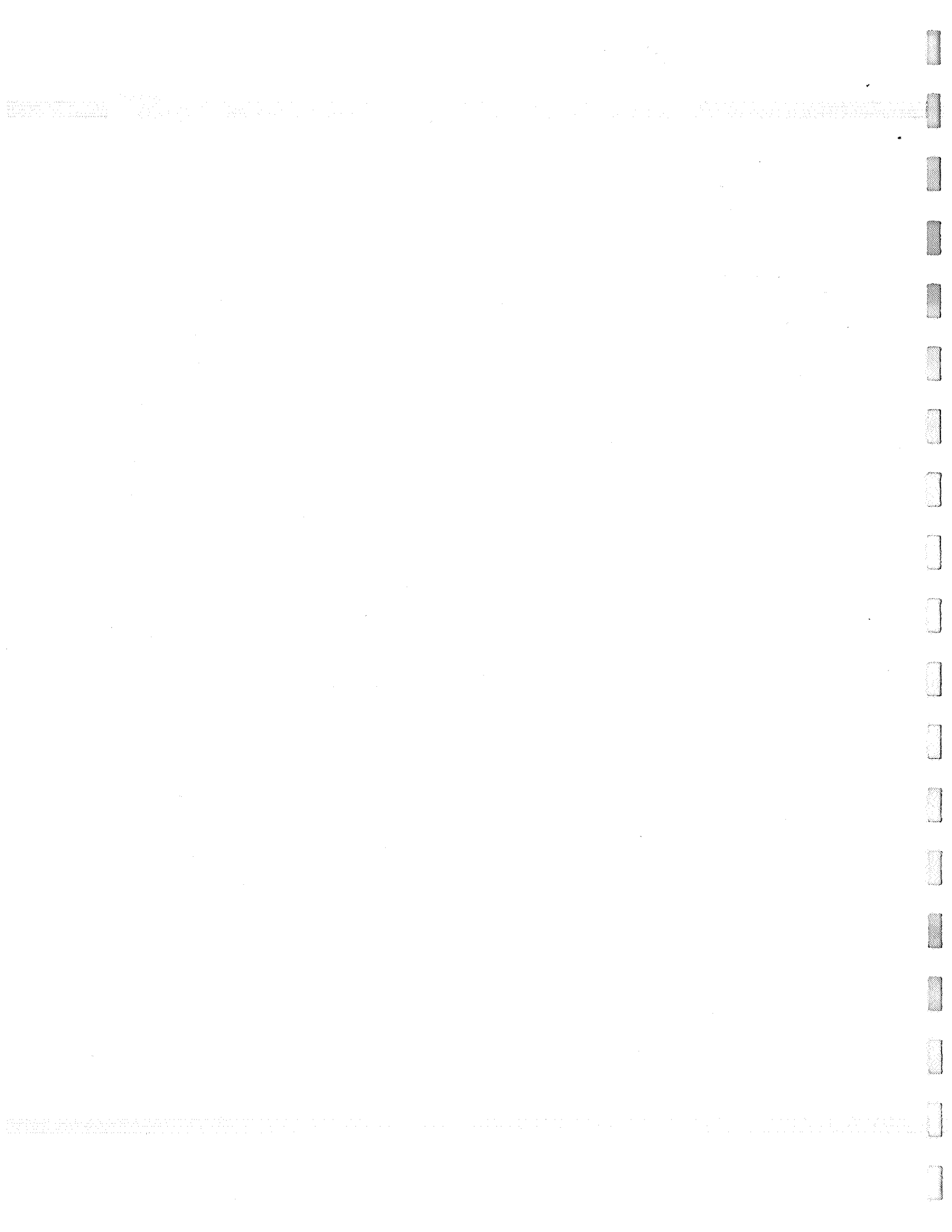
ABSTRACT

This is a final report defining the results of a development program to upgrade the performance of the Bendix J-2 pneumatic gimbal actuator.

The pneumatic gimbal actuator was upgraded by replacing the vane type servomotor with a higher performance gear type servomotor. The gear servomotor was designed to meet the requirements of NASA Specification 50M35026 entitled "Pneumatic Actuator, Thrust Vector Control System, Design Specification For."

The gear servomotor's performance was demonstrated on the existing gimbal actuator with hydrogen gas at -250°F and 800 psig supply pressure. The performance improvement over the vane servomotor was achieved as predicted. The frequency response of the actuator driving a simulated load was improved to over 10 cps from the original vane motor's 3 cps. The new servomotor's performance was further demonstrated by running all of the performance tests required by the above specification, and the results are included in this report.

The conclusions of this program confirm that a pneumatic gimbal actuator unlimited by operating temperature can perform to the J-2 engine requirements.



FOREWORD

This report was prepared by the Bendix Research Laboratories under NASA Contract NAS 8-5407, Modification No. 10, Phase I.

This work was sponsored by the Flight Controls Development Branch, Astrionics Division, National Aeronautics and Space Administration, Marshall Space Flight Center, Huntsville, Alabama. The program was administered under the direction of Mr. J. Peoples and Mr. J. Smith, Code R-ASTR-NRM, NASA. The work was conducted at the Bendix Research Laboratories in the Energy Conversion and Dynamic Controls Laboratory, managed by Mr. L. B. Taplin. The project was directed by Mr. K. W. Verge, Department Head, Flight Controls Department, with Mr. M. H. Cardon, Project Engineer, assigned as servomotor design supervisor and Mr. G. I. Boyadjieff, Project Engineer, assigned as actuator supervisor.

SECTION 1
INTRODUCTION AND SUMMARY

This report summarizes the results of a development program to upgrade the performance of the Bendix J-2 pneumatic actuator. This phase of the J-2 actuator program was concerned with replacing the existing vane servomotor with a gear servomotor.

This program was sponsored by the Flight Control Development Branch, Astrionics Division, National Aeronautics and Space Administration, Marshall Space Flight Center, Huntsville, Alabama under Contract No. NAS 8-5407, Modification No. 10, Phase I.

The new gear servomotor, together with the servovalve, is shown in Figure 1-1. Figure 1-2 shows the servomotor installed on the J-2 actuator. The servomotor was designed to meet the requirements of NASA Specification 50M35026, entitled "Pneumatic Actuator, Thrust Vector Control System, Design Specification For."

The basic design of the gear servomotor is a three-gear symmetrical motor ported so that supply and exhaust pressures can be alternated by the servovalve to obtain equal performance characteristics in both directions of rotation. The developed stall torque is 300 lb-in at 800 psig supply pressure to the servovalve and the peak horsepower is 13.5 hp with a torque efficiency of 85%. These performance values result in the gimbal actuator characteristics listed below:

Force output	42,000 lb
Force at 1.65 in/sec	23,200 lb
Slew Speed	3.3 in/sec
Frequency response	-3 db @ >10 cps

The frequency response performance represents a significant improvement over the existing vane type servomotor response of -3 db at 3 cps.

The purpose of the program has been accomplished with the demonstration of the performance of the pneumatic gear servomotor.

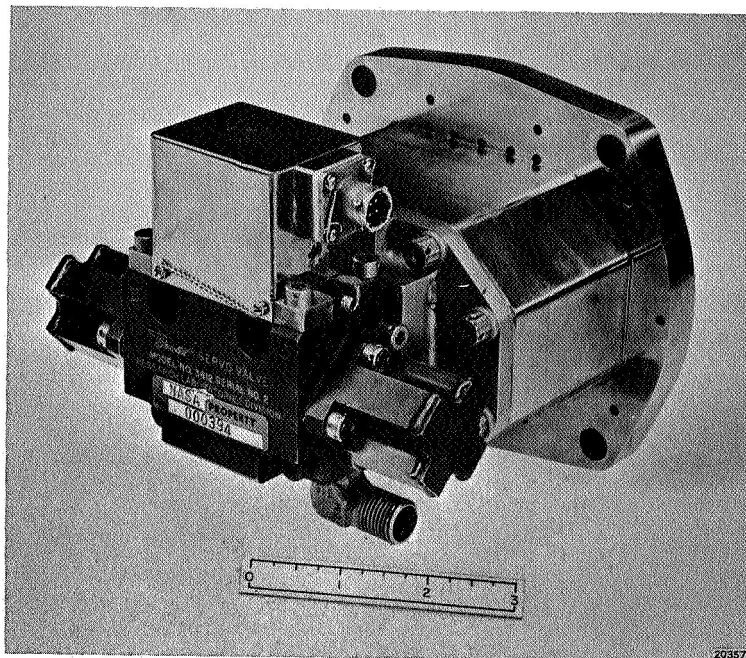


Figure 1-1 - Pneumatic Gear Type Servomotor and Servovalve
(Viewed from Servovalve End)

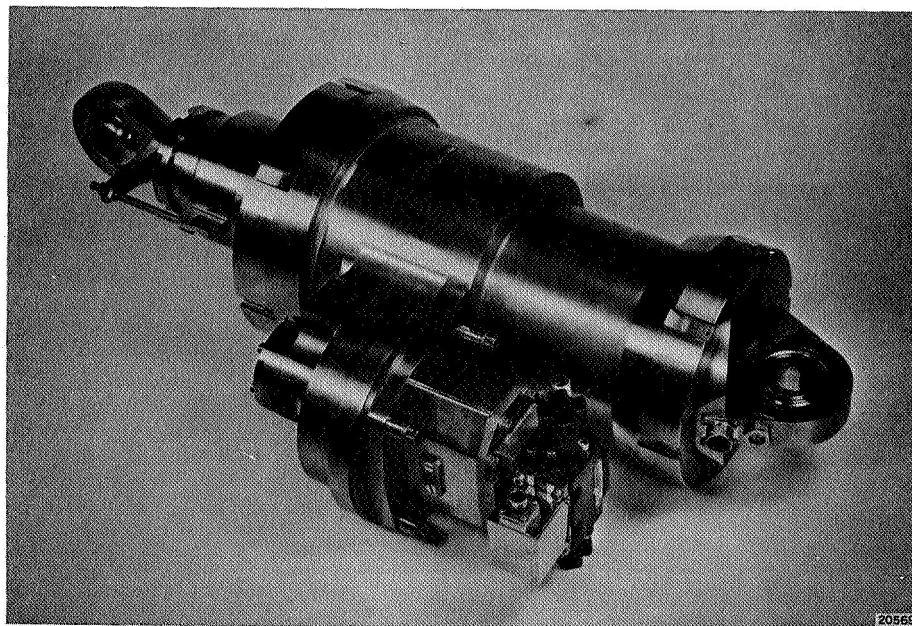


Figure 1-2 - J2 Engine Pneumatic Gimbal Actuator

SECTION 2

SERVOMOTOR DEVELOPMENT

Presented in this section are the results of the development of a gear type servomotor to mate with the NV-B1 gimbal actuator. The servomotor is described, and the analysis conducted to establish performance requirements and motor design details is presented. Servomotor test results are also presented.

2.1 DESCRIPTION

The gear type servomotor consists of a Bendix Research Laboratories servovalve Model No. 3812 and a three-gear pneumatic motor. It is designed to operate with hydrogen as the supply gas at a pressure of 800 psig and through a temperature range of 150°F to -250°F. Photographs of the servomotor without its cover are shown in Figure 2-1. Performance characteristics of the servomotor are summarized in Table 2-1. Some of the data presented is for nitrogen supply gas because a substantial amount of the development was conducted using this gas.

Table 2-1 - Servomotor Performance Characteristics

Characteristic	Units	Nitrogen 40°F	Hydrogen 40°F
Maximum Torque	lb-in	298-288	297-295
Torque Sensitivity	lb-in/amp	37,500	34,500
Speed Sensitivity	rpm/amp	375,000	1,060,000
Horsepower		4.8	13.5
Hysteresis - Output Shaft Locked at Zero Torque	ma	0.5	1.0
Hysteresis - Free Running at Zero Speed	ma	0.25	0.25
Specific Gas Consumption	lb/hp-hr	184	15
Torque Efficiency	%	84	85
Natural Frequency	cps	28	—

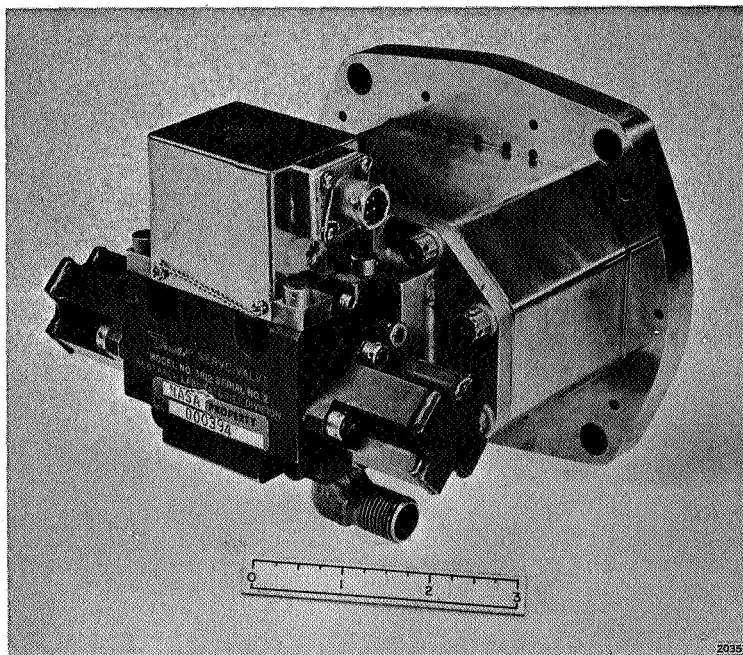
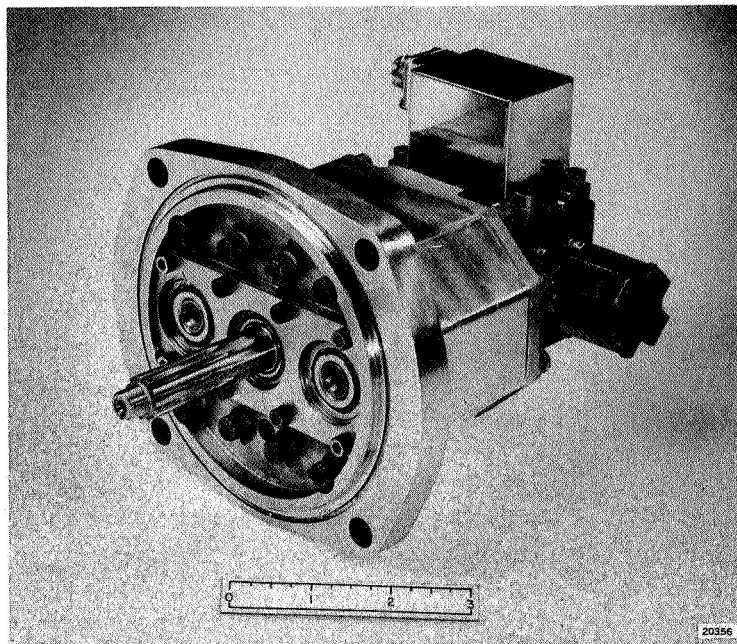


Figure 2-1 - Pneumatic Gear Type Servomotor and Servovalve
(Viewed from Output Shaft End)

2.1.1 Servo Valve Model 3812

The Model 3812 servo valve is a two-stage electropneumatic four-way spool valve. It is the same valve that was used with the vane type servomotor with the exception that the spool has been replaced with one that, when mated with the valve body, has a zero lap on both the supply land and exhaust land; as a result, the supply and exhaust metering areas are equal. The servo valve is actuated by a 250-milliwatt signal applied to a dry-coil-type torque motor. A ± 50 -milliampere current signal displaces the 0.625-inch diameter spool ± 0.015 inch, in a direction dependent upon applied current polarity. The spool supply and exhaust metering areas are 0.0186 in². The valve body and spool material is 440C stainless steel with a black oxidized surface per MIL-0-13924A, Class 2. The valve is shown in Figures 2-2 and 2-3.

The torque motor is of the permanent magnet type and is supplied by Midwestern Instruments, Incorporated, as Model 39-4 and by Servotronics, Incorporated, as Model 29-2-32. The coil resistance of the torque motors is 100 ohms.

2.1.2 Gear Motor Design

The three-gear pneumatic motor, of which a section view is shown in Figure 2-4, has a theoretical displacement of 3.16 in³/rev. The motor is face-mounted on the actuator so that the input pinion gear of the actuator's planetary transmission is assembled directly onto the output shaft of the motor. All exhaust gas is ported through the front mounting face, and a seal in this face prevents leakage of the exhaust gas to the atmosphere.

A cover is placed over the motor to capture leakage gas from the motor and direct it through the mounting face. The cover is provided with an expansion joint to allow for differing expansions when extreme temperature changes take place. A manifold plate, which contains the supply inlet port, is mounted on the rear face of the motor, and the servo valve is mounted on this plate.

The output gear of the motor is slightly larger than the two pinion gears, having 15 teeth as compared with 12 for the pinions. The gears are supported radially by radial contact ball bearings and are held axially by carbon side plates that form a sealing surface with the sides of the gears.

A more detailed description of the motor is presented in the following subsections.

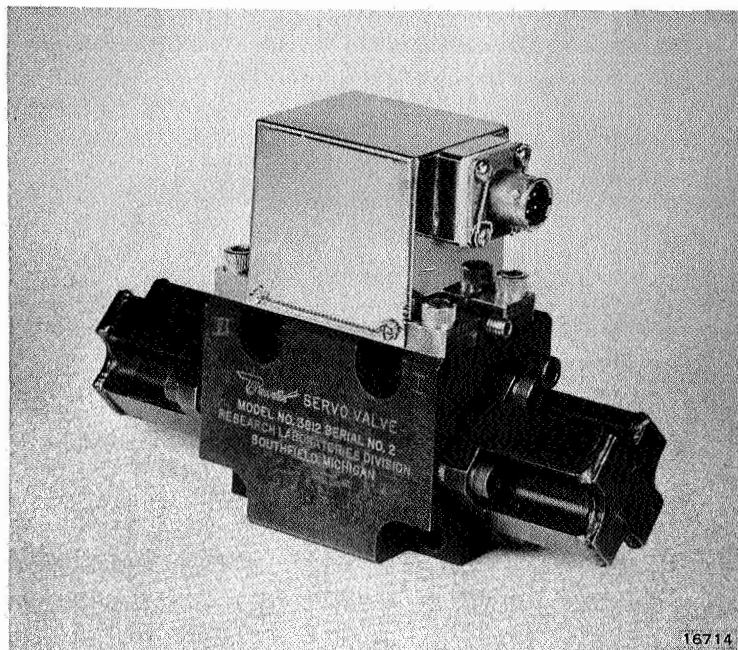


Figure 2-2 - Bendix Servo Valve Model 3812 Servo Valve

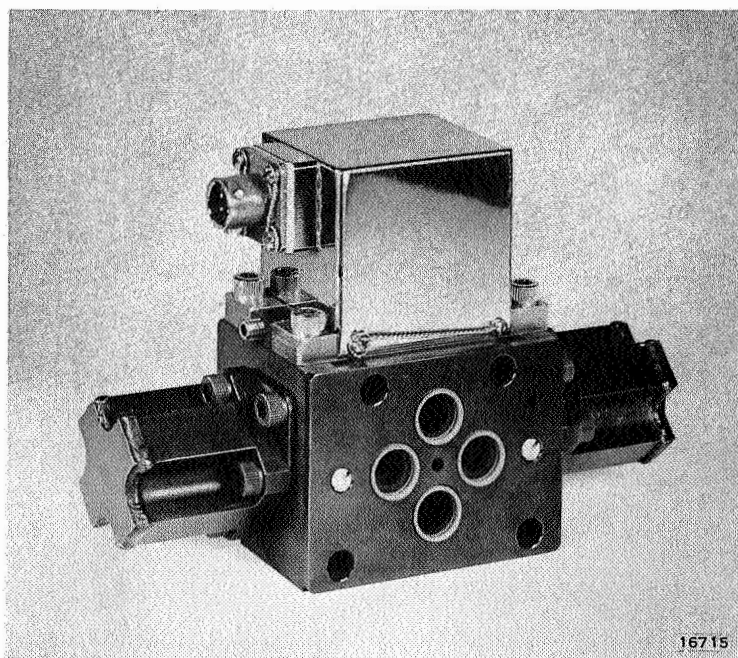
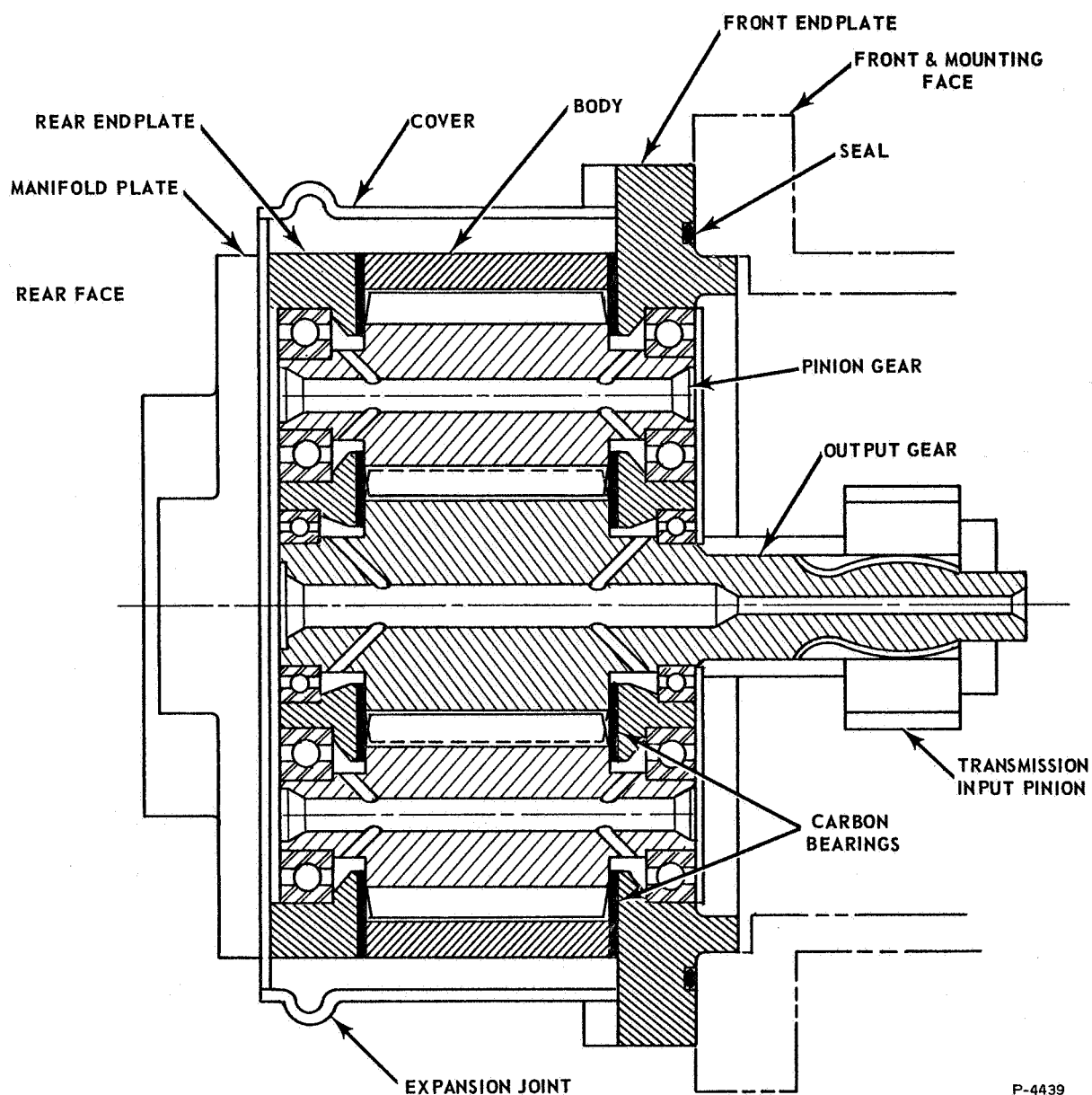


Figure 2-3 - View of Servo Valve Showing Ports



P-4439

Figure 2-4 - Section View of Gear Motor

2.1.2.1 Motor Gears

The three motor gears (output gear and two pinions) have the following dimensions:

Diametral Pitch	10
Pressure Angle	30 degrees
Addendum	0.100 inch
Dedendum	0.125 inch
Face Width	1.560 inches
Pitch Diameter	
Output Gear	1.500 inches
Pinion	1.200 inches
Number of Teeth	
Output Gear	15
Pinion	12

The gears are made of 440C stainless steel and hardened to Rockwell "C" 50-55. The gear teeth faces are coated 0.0002-inch to 0.0005-inch thick with a proprietary dry-film lubricant, Magnaplate Hi-T-LUB.

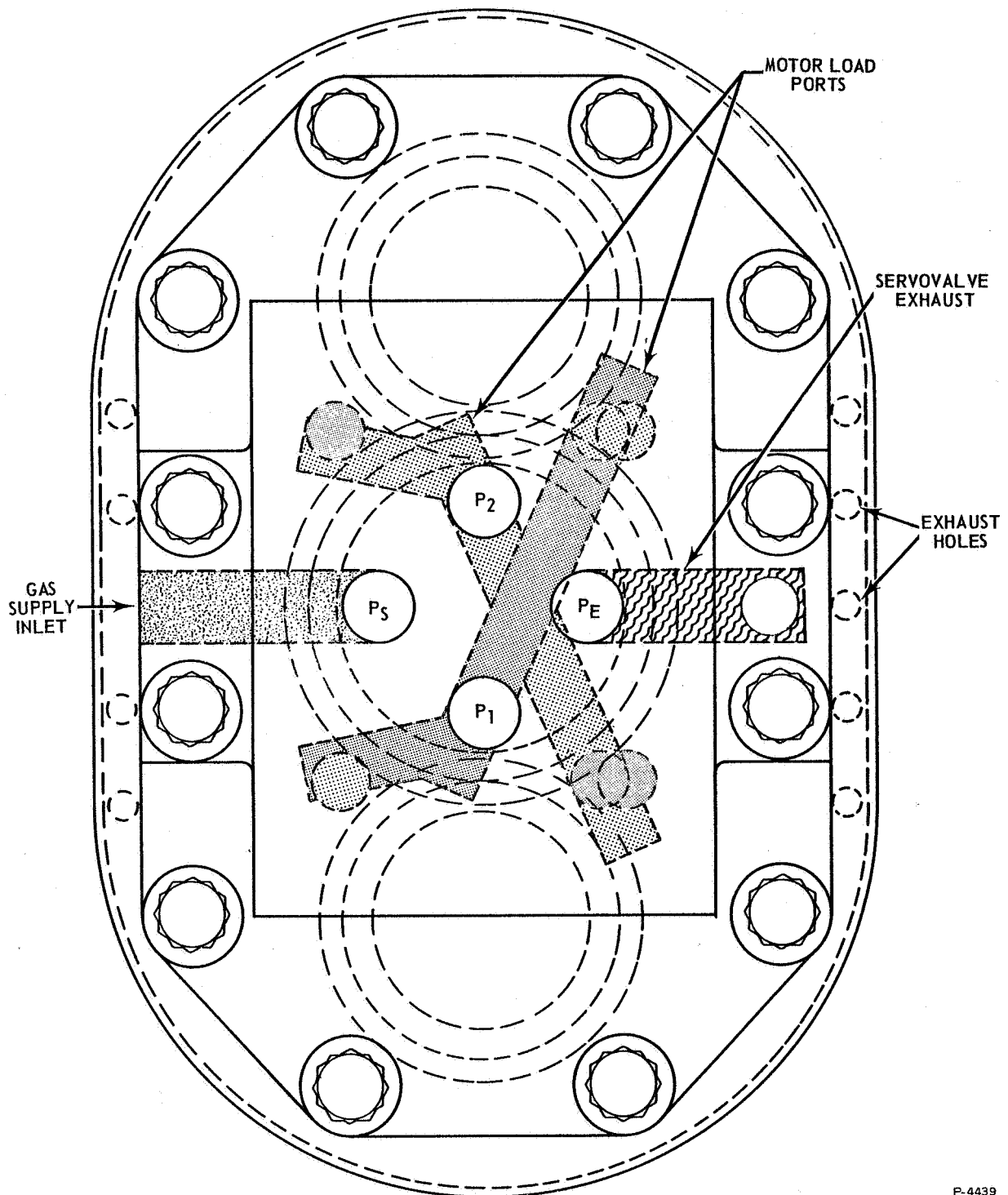
2.1.2.2 Bearings

The radial loads are carried by ball bearings. These bearings are of the split race type, made of 440C stainless steel, and have a separator made of Dupont SP-3.

The axial loads on the gears are carried by the carbon-graphite end plates that are bonded to the front and rear end plates. The bearing surface between the gear and carbon also forms a dynamic seal. The carbon-graphite material is manufactured by the Pure Carbon Company and is designated as Purebon P-5-N. The carbon graphite was bonded to the stainless-steel end plates using a thixotropic epoxide adhesive. This adhesive is made by Emerson & Cuming, Incorporated, and is sold under the trade name Eccobond 285. Their catalyst 24LV was used in the bonding process. The results of tests of shear strength at cryogenic temperatures and the effects of immersing samples in liquid nitrogen are presented in Appendix A.

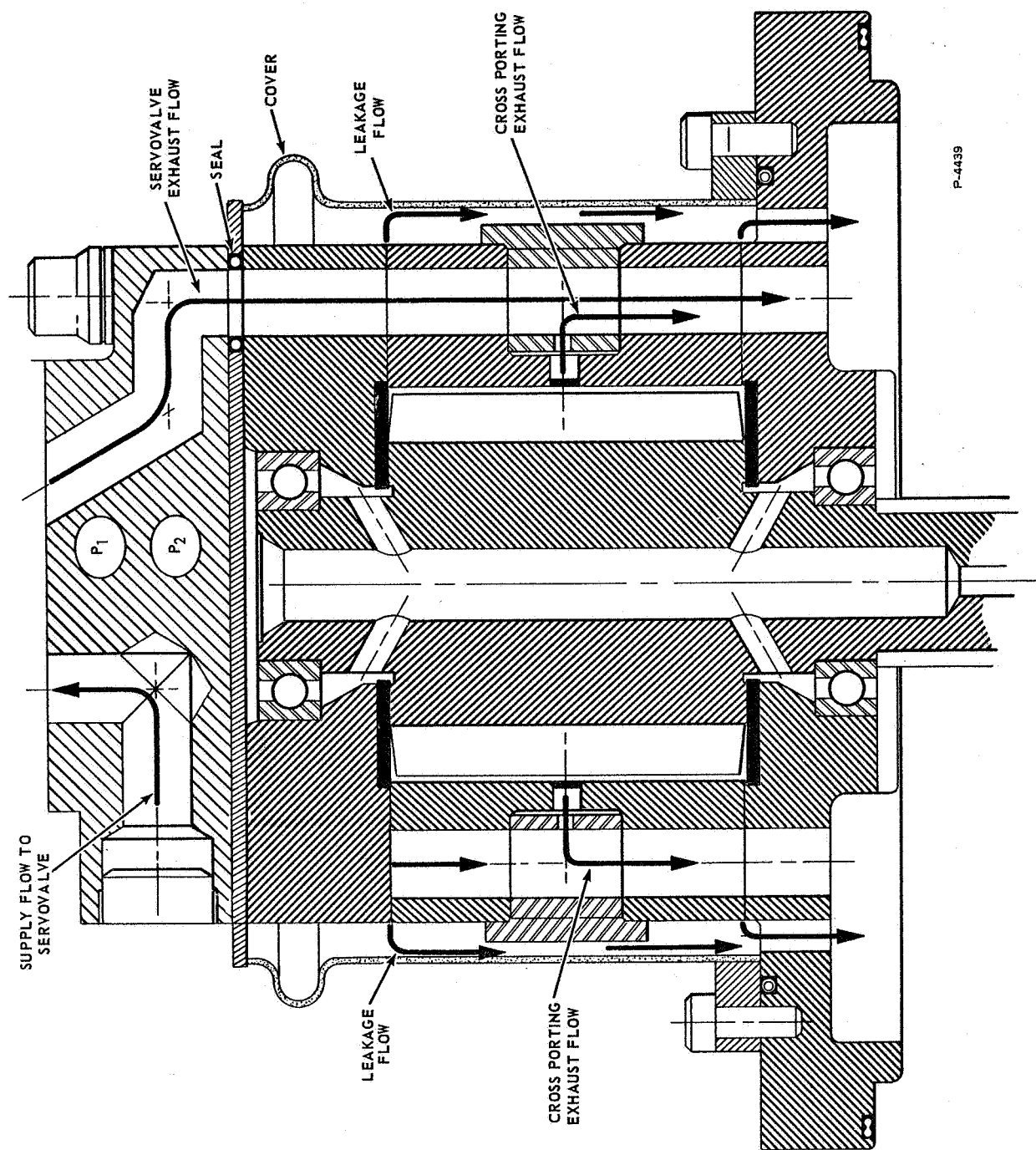
2.1.2.3 Manifolding

The servovalve interface is on the manifold plate that is mounted to the rear face of the motor. The supply gas is brought in through this manifold plate to the servovalve. The valve interface, supply manifold, load port (P_1 and P_2) manifold and exhaust manifold from the servovalve are illustrated in Figure 2-5. Also shown in this figure is the location of the exhaust holes in the front end plates through which the leakage flow of the motor is directed. Figure 2-6 shows how the exhaust flow from the servovalve and from cross-porting is manifolded.



P-4439

Figure 2-5 - Supply, Load Ports, and Exhaust Manifolds
at Servovalve Interface



P-4439

Figure 2-6 - Exhaust Flow Manifolding

2.1.2.4 Pressure Balancing

The motor gears are held axially by carbon plates which are bonded to the front and rear end plates. Since the motor gears rotate at a comparatively high speed, loads on the carbon plates must be kept low in order that satisfactory life characteristics can be achieved. A major source of axial loads is the pressure differentials existing across the sides of the gears. To keep these loads to a minimum, the sealing surfaces on both sides of the gear are made exactly alike (see Figure 2-7), and the gas leaking past the gears is ported to exhaust through adequately sized passages.

2.1.2.5 Cross-Porting

To increase the maximum horsepower and speed of a motor-valve combination, the motor is cross-ported. To cross-port a motor, an orifice to exhaust is placed at some point between the load ports, P_1 and P_2 , and on a surface enclosing a rotating member carrying the flow being displaced from the load port that is under pressure to the load port that is open to exhaust. (In this case the rotating member is the output gear.) While the motor is running, the orifice exhausts a portion of the gas (depending upon orifice size) being carried between the load ports, P_1 and P_2 , thus reducing the amount of gas that must be exhausted through the servovalve exhaust orifice. This reduction in flow reduces the pressure of the load port being exhausted, increasing the differential pressure generated at a given speed, thus increasing output horsepower. As a result of the porting, the load port pressures, P_1 and P_2 , equalize at a higher speed, increasing the maximum speed of the motor. The cross-porting orifice is sized to give the desired torque-speed characteristics. Figure 2-8 illustrates how the gear motor is cross-ported. In the cross-porting of this motor, orifices are removable and placed on opposite sides of the output gear. Being removable, the orifice may be experimentally sized to give desired performance characteristics.

2.1.2.6 Material

The motor is constructed principally from Martensitic and Ferritic (400 series) stainless steels. The gears, as mentioned before, are made from 440C and hardened to Rockwell "C" 50-55. The body, end plates, and manifold are made from 416 stainless steel and hardened to Rockwell "C" 38-41. In the annealed condition, this steel consists of ferrite and carbides. In the hardened condition, the structure is Martensitic. Sulfur has been added to this steel to impart free-machining properties. The cover is of a silver-brazed construction and is made from half-hard SAE 70 brass sheet and 416 stainless steel. The flange containing holes for the mounting screws is made of 416 stainless steel.

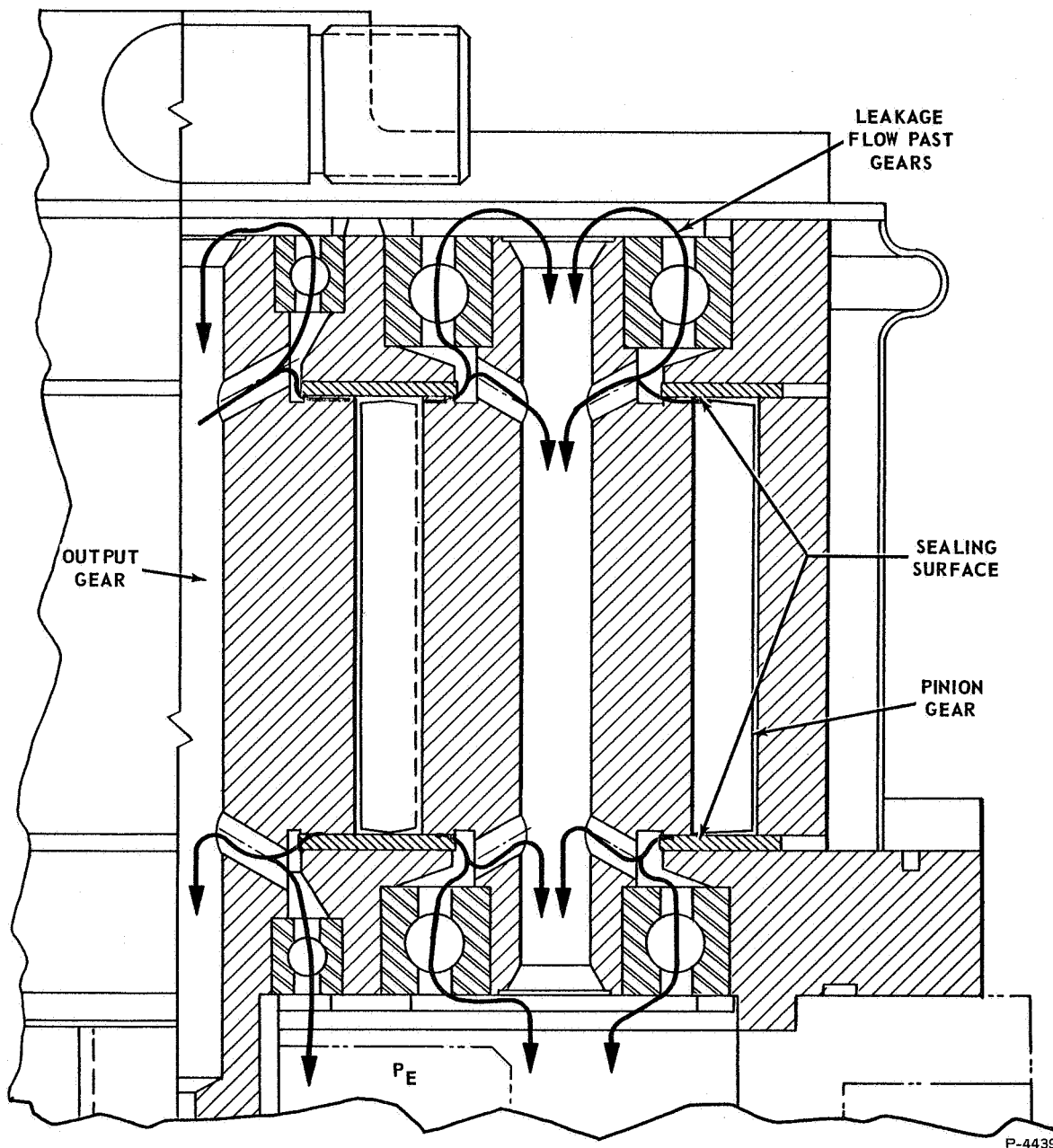


Figure 2-7 - Pressure Balancing and Exhausting of Leakage Flow Past Sides of Gears

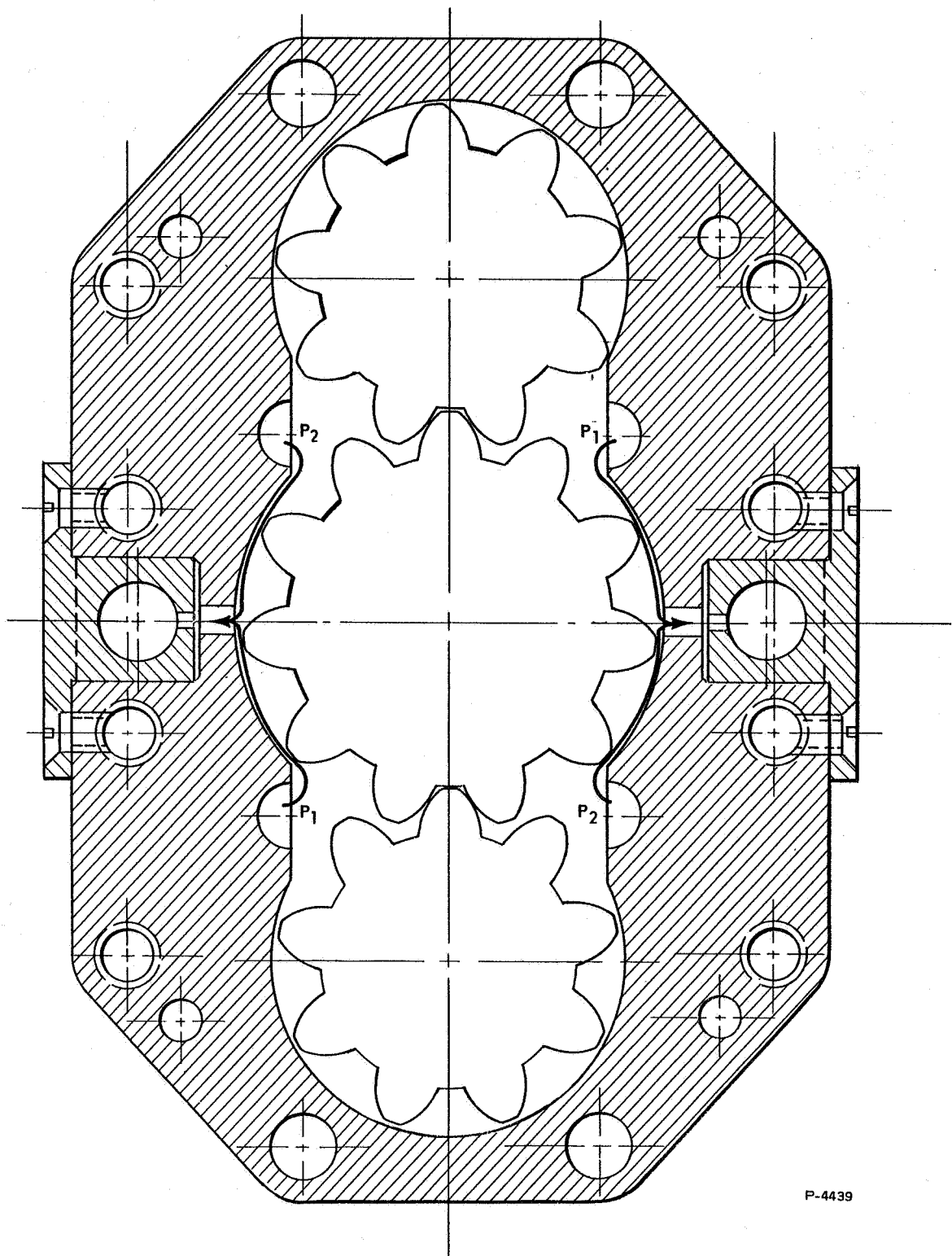


Figure 2-8 - Cross-Porting Between Load Port Pressures P_1 and P_2

2.2 ANALYSIS

The performance and design analysis associated with the developmental gear-type servomotor are presented in this section. In the performance analysis, servomotor performance requirements are defined and theoretical motor displacement and performance characteristics are established. In the design analysis, bearing loads, gear tooth stresses, and shaft bending and torsional stresses are determined.

2.2.1 Performance

The NV-B1 gimbal actuator performance requirements are listed in Table 2-2 alongside the servomotor requirements (which are defined from the actuator requirements). The motor displacement and design were established from these requirements. The theoretical performance characteristics of the servomotor are presented in the last column of Table 2-2.

2.2.1.1 Torque-Speed Requirements

The torque-speed requirements of the motor are established from the stall torque, maximum speed, frequency response, and rated load-speed requirements of the actuator.

The actuator stall torque, maximum speed, and rated load-speed requirements are converted to motor torque-speed requirements by using the transmission and ball screw ratio of 221 radians per inch and an efficiency of 72%. These requirements are shown graphically in Figure 2-9. Torque-speed requirements to meet frequency response are established as follows.

Required motor torque as a function of acceleration is given by the equation:

$$T_m = \left(J_m + \frac{J_1}{e_1} + \frac{J_2}{e_1 e_2} \right) \alpha_m + \frac{T_L}{e_1 e_2} \quad (1)$$

where

T_m = torque output of motor (lb-in)

α_m = angular acceleration of motor (rad/sec²)

J_m = motor and planetary input gear inertia
= 0.00304 lb-in-sec²

J_1 = ball nut and planetary output inertia reflected
to the motor = 0.0007 lb-in-sec²

Table 2-2 - Actuator Performance Specifications, Servomotor Requirements and Theoretical Gear Motor Performance

Performance Characteristics	Actuator Specification	Servomotor Requirement	Theoretical Gear Motor Performance
Maximum Stall Force	42,000 lb	264 lb-in	264 lb-in at 800 psi
Rated Load-Speed	23,200 lb at 1.66 in/sec	145 lb-in at 3500 rpm	200 lb-in at 3500 rpm
Maximum No-Load Speed	3.45 in/sec	7000 rpm	13,500 rpm at -250°F 21,200 rpm at 60°F Maximum actuator speed to be limited by actuation system compensation.
Acceleration	$\geq 21 \text{ in/sec}^2$ $< 59.5 \text{ in/sec}^2$	$\geq 4640 \text{ rad/sec}^2$ $< 13,100 \text{ rad/sec}^2$	32,600 rad/sec ² at 850 psi 31,600 rad/sec ² at 800 psi
Closed-Loop Frequency Response (7300-lb friction 116.5 lb-sec ² /in inertia) Input signal $\pm 0.05 \text{ in}$.	8 cps	-----	-----
Supply Gas	Hydrogen Pressure: 800 ± 50 psi Temperature 60°F to -250°F	-----	-----

P-4439

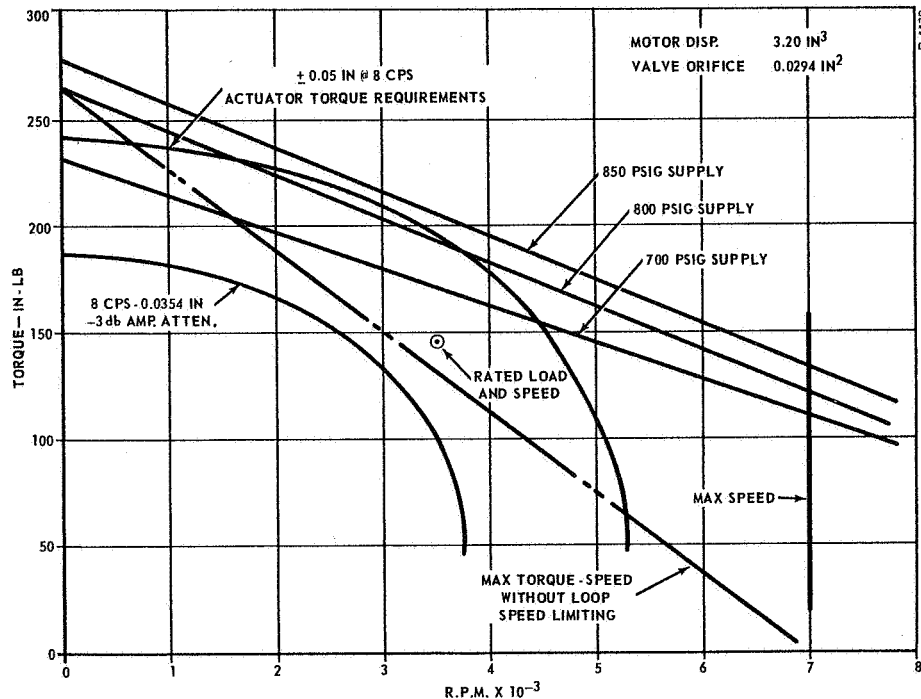


Figure 2-9 - Predicted Servomotor Performance

J = load inertia reflected to the
motor = 0.00239 lb-in-sec²

T_L = frictional load at motor = 33 lb-in

e₁ = efficiency of transmission = 0.90

e₂ = efficiency of ball screw = 0.80

$$T_m = 7.14 \times 10^{-3} \alpha_m + 46 \text{ (lb-in)} \quad (2)$$

Motor acceleration when responding sinusoidally is given by the expression

$$\alpha = -A\omega^2 \sin \omega t \quad (3)$$

where

α = motor acceleration (rad/sec²)

A = amplitude of motion (rad)

ω = frequency (rad/sec)

t = time (sec)

For 8 cps response and a 0.05-inch actuator
amplitude,

$$\alpha = -0.05 \times 221 (2\pi 8)^2 \sin \omega t$$

$$\alpha = -27,800 \sin \omega t \quad (4)$$

For 8 cps response and a 0.035-inch (-3 db attenu-
ation) amplitude,

$$\alpha = -19,500 \sin \omega t \quad (5)$$

By substituting equations (4) and (5) into (2), motor torque as a function
of ωt can be established for output amplitudes of 0.05 and 0.035 inch.

The motor's angular velocity, as a function of ωt , is calculated from the equation

$$\dot{\theta} = A\omega \cos \omega t \quad (6)$$

where

$\dot{\theta}$ = angular velocity of the motor (rad/sec)

For 8 cps response and a 0.05-inch amplitude,

$$\dot{\theta} = 556 \cos \omega t \quad (7)$$

For 8 cps response and a 0.035-inch amplitude,

$$\dot{\theta} = 389 \cos \omega t \quad (8)$$

Values of torque as a function of ωt , and corresponding velocities, are calculated from the preceding equation for amplitudes of 0.05 and 0.035 inch. The resulting curves are shown in Figure 2-9.

It can be seen in Figure 2-9 that, if the actuator is to meet 8-cps bandwidth without any attenuation of its output motion, the motor must exceed the specified rated load-speed characteristics. Also, the motor acceleration requirements are 27,800 rad/sec² for an output amplitude of 0.05 inch at 8 cps and 19,500 rad/sec² for an output amplitude of 0.035 inch. The limits of load acceleration, as specified in the actuator specification, are 21 in/sec² minimum to 59.5 in/sec² maximum. These values convert to motor accelerations of 4640 rad/sec² and 13,100 rad/sec², respectively. These specified values are not consistent with the specified response characteristics.

2.2.1.2 Motor Displacement

Having established the required torque-speed characteristics, the next step is to define the motor displacement. The displacement per revolution of the motor (D_m) as a function of motor torque (T_m) is given by the following expression:

$$D_m = \frac{2\pi T_m}{P_1 - P_2} \quad (9)$$

Previous experience with pneumatic actuator systems has shown that $(P_1 - P_2)$ at stall conditions is a function of the supply pressure, the ratio of effective leakage area to valve orifice area, and the exhaust porting. If the leakage area is assumed proportional to the motor displacement, $(P_1 - P_2)$ can be estimated for a given valve and gear motor combination by comparing the ratios of motor displacement to the comparable valve opening (A_v). A comparison of two gear-type servomotors is given in Table 2-3 below. A ratio of $(P_1 - P_2)/P_s$ of 0.65 was selected for determining the displacement of the motor in this case.

Table 2-3 - Displacement/Area Ratio and Pressure Ratio Comparison

Servomotor	A_v in^2	D_m in^3/rev	D_m/A_v in/rev	P_s psi	$(P_1 - P_2)$ psi	$\frac{P_1 - P_2}{P_s}$
N	0.0065	0.85	131	200	140	0.65
P	0.028	3.75	134	700	420	0.60

The displacement of the motor is sized to meet the maximum actuator stall force, (F_a) .

$$T_m = \frac{F_a}{R \times \eta} = \frac{42,000}{221 \times 0.72} = 265 \text{ lb-in} \quad (10)$$

where

R = transmission ratio (rad/in)

η = transmission efficiency (assume 72%)

Thus, from equation (9),

$$D_m = \frac{2\pi T_m}{P_1 - P_2} = \frac{2\pi \times 265}{(0.65)(800)}$$

$$= 3.2 \text{ in}^3/\text{rev.}$$

2.2.1.3 No-Load Speed

The maximum speed of the motor is calculated from the following relationship:

$$N_m = \frac{Q_m}{D_m} \quad (11)$$

where

N_m = maximum motor speed (rpm)

Q_m = volume flow through motor (in³/sec)

It is assumed that the motor is ideal and that the motor port pressure is one-half the supply pressure (400 psi). The motor port pressure assumption is made on the basis of previous motor test results. In a fairly tight motor, it is actually set by the amount of cross-porting in the motor. (See Section 2.1.2.5.)

The weight flow through the valve is calculated from the expression for gas weight flow out of an upstream region based upon upstream conditions:

$$W = C_d A_o \frac{P_u}{\sqrt{T_u}} C_2 \left[f_1 \left(\frac{P_d}{P_u} \right) \right] \quad (12)$$

where

W = gas flow (lb/sec)

C_d = orifice discharge coefficient = 0.8

A_o = orifice area (in²) = 0.0294

C_2 = gas coefficient (hydrogen) = 0.1393

P_u = supply pressure (psi) = 800

P_d = motor port pressure (psi) = 400

T_u = gas temperature = 210°R

$$f_1 = \left(\frac{P_d}{P_u} \right) = f_1 \left(\frac{400}{800} \right) = 1 \text{ (assume sonic flow)}$$

$$W = 0.8 \times 0.0294 \times \frac{800}{\sqrt{210}} \times 0.1393 \times 1$$

$$= 0.181 \text{ lb/sec}$$

The gas volume flow through the valve is calculated from:

$$Q_u = C_d A_o \sqrt{T_u} R C_2 \left[f_1 \left(\frac{P_d}{P_u} \right) \right] \quad (13)$$

where

Q_u = volume flow based on upstream conditions (in^3/sec)

R = gas constant (hydrogen) = 9270

$$Q_u = 0.8 \times 0.0294 \sqrt{210} \times 9270 \times 0.1393 \times 1$$

$$= 442 \text{ in}^3/\text{sec}$$

After passing through the servovalve, the gas expands adiabatically before flowing through the motor.

$$Q_m = \frac{Q_u}{\left(\frac{P_m}{P_u} \right)^{\frac{1}{k}}} \quad (14)$$

where k is the ratio of specific heats of hydrogen and equal to 1.41.

$$\therefore Q_m = 724 \text{ in}^3/\text{sec}$$

The motor no-load speed with a supply gas temperature of -250°F from equation (11) is

$$N_m (-250^{\circ}\text{F}) = \frac{724 \text{ in}^3/\text{sec}}{3.2 \text{ in}^3/\text{rev}} \times 60 \frac{\text{sec}}{\text{min}} = 13,500 \text{ rpm}$$

No-load speed with a supply gas temperature of 60°F is

$$N_m (60^{\circ}\text{F}) = 13,500 \times \sqrt{\frac{520}{210}} = 21,200 \text{ rpm}$$

2.2.2 Design

In the preceding text, it was established that a motor with displacement of $3.2 \text{ in}^3/\text{rev}$ was required to drive the actuator. An equation for motor displacement in the terms of various design parameters is derived in Appendix B and given below:

$$D_m = 2\pi \ell \left[\left(r_1^2 - R_1^2 \right) + \frac{R_1}{R_2} \left(r_2^2 - R_2^2 \right) \right] \quad (15)$$

where

ℓ = length of the gears (inch)

r_1 = outer radius of output gear (inch)

R_1 = pitch radius of output gear (inch)

r_2 = outer radius of pinion gear (inch)

R_2 = pitch radius of pinion gear (inch)

$$r_1 = R_1 + a \quad (16)$$

and

$$r_2 = R_2 + a \quad (17)$$

where

a = addendum of the gear tooth

For a full-depth tooth,

$$a = \frac{1}{P_D} \quad (18)$$

where

D = diametral pitch of the gear

Substituting equations (16) and (17) into (15),

$$D_m = 2\pi \ell \left[4 a R_1 + a^2 \left(1 + \frac{R_1}{R_2} \right) \right] \quad (19)$$

Substituting equation (18) into (19),

$$D_m = 2\pi \ell \left[\frac{4 R_1}{P_D} + \frac{1}{P_D^2} \left(1 + \frac{R_1}{R_2} \right) \right] \quad (20)$$

Equation (20) expresses motor displacement in terms of diametral pitch, length, and the pitch radii of pinion gear and output gear. There are constraints that must be considered in arriving at values for these parameters. The constraints are the required package size, maintaining a reasonable gear length-to-diameter ratio, achieving a low motor inertia; in addition, in order to keep the pinion gear rotational velocity at a practical value, the ratio of the pitch radius of the output gear to the radius of the pinion gear must be kept low. The final selected values for parameters of equation (20) and the motor displacement are:

$$P = 10$$

$$R_1 = 0.750 \text{ inch}$$

$$R_2 = 0.5625 \text{ inch}$$

$$\ell = 1.560 \text{ inches}$$

$$D_m = 3.16 \text{ in}^3/\text{rev}$$

2.2.2.1 Bearing Loads and Stresses

The only moving parts of the gear motor are the gears and they are supported axially by carbon plates and radially by ball bearings. As a result of pressure balancing, the axial loads on all of the gears and the radial loads on the output gear are very low and are not considered in this analysis. The radial loads on the pinion gears are due to the load pressures, P_1 and P_2 , acting on the projected area of the pinion gear. The radial load on each of the two bearings supporting the pinion gear is given by the expression:

$$F_B = \frac{(P_1 + P_2) A_P}{4} \quad (21)$$

where

F_B = radial bearing load (lb)

A_P = projected area of the pinion gear (in.)

P_1 and P_2 = load port pressures (psi)

The mean compressive stress in the balls of a bearing is determined from the equation:

$$S_m = 15,079 \frac{\left[\frac{1}{R_{a1}} + \frac{1}{R_{a2}} + \frac{1}{R_{b1}} + \frac{1}{R_{b2}} \right]^{2/3}}{\mu \nu} P_O^{1/3} \quad (22)$$

where

R_{a1} and R_{a2} = principle radii of curvature of ball (in.)

R_{b1} and R_{b2} = principle radii of curvature of inner race (in.)

P_O = normal load (lb)

μ and ν = hertz factors

P_O is established from the equation

$$P_O = 4.37 \frac{F_B}{\text{number of balls in bearing}} \quad (23)$$

A split-race ball bearing was selected for use in this application because a greater number of balls can be used, increasing the load carrying capacity of a bearing of given inner and outer diameter. The balls and races of the bearing are made of 440C stainless steel. The separator is made of Dupont SP-3 and provides the necessary bearing lubrication.

For the bearing size selected, the mean compressive stress is equal to:

$$S_m = 54,400 P_0^{1/3} \quad (24)$$

In Table 2-4, bearing loads and mean compressive stresses for various motor speeds are presented. The bearing loads are derived from the torque curve of the motor.

Table 2-4 - Bearing Loads and Stresses for Various Motor Speeds

Pinion Speed rpm	Bearing Load (F_B) lb	Bearing Mean Compressive Stress psi
Stall	350	290,000
3750	153	221,000
4400	153	281,000
8750	110	267,000

Bearing loads and speeds are in line with bearing practice for the bearing material, lubricant and environment of this application. Bearings of the type described have operated successfully under the specified conditions in the NV-B1 actuator transmission.

2.2.2.2 Gear Tooth Stress Analysis

The gear tooth size and face width were selected to achieve the desired motor displacement and, as a result, the gear teeth are relatively large in comparison with the loads they must carry. Gear tooth beam stresses and contact stresses are low. The low contact stress should yield good wear characteristics.

The maximum tooth beam stress is calculated by using the Lewis equation:

$$F_T = \frac{S_B \ell Y}{P} \quad (25)$$

where

F_T = tangential tooth load (lb)

S_B = maximum tooth bending stress (psi)

ℓ = tooth face width = 1.56 in.

Y = tooth form factor = 0.349

P = diametral pitch = 10

The maximum tooth load is calculated from the following:

$$E_T = \frac{T_m}{2 R_o} \quad (26)$$

where

T_m = motor output torque = 265 lb-in

R_o = major radius of output gear = 0.85 in.

$$F_T = 156 \text{ lb}$$

Substituting into equation (25) and solving for the beam stress,

$$S_B = \frac{156 P}{\ell Y} \quad (27)$$

Substituting the proper values in equation (27):

$$S_B = 2860 \text{ psi}$$

The tooth contact stress (S_g) is calculated from the following expression where the gear and pinion are of the same material:

$$S_g = \sqrt{\frac{0.35 F_m E \left(\frac{1}{R_1 \sin \phi} + \frac{1}{R_2 \sin \phi} \right)}{2\ell}} \quad (28)$$

where

F_m = maximum contact force = $F_T / \cos \phi$ (lb)

E = Young's modulus = 29×10^6 (psi)

R_1 and R_2 = pitch radii of gears (in.)

ϕ = pressure angle = 30 deg

l = gear face width (in.)

$$S_g = \sqrt{\frac{0.35 \times 180 \times 29 \times 10^6 \left(\frac{1}{0.375} + \frac{1}{0.28} \right)}{2 \times 1.56}}$$

$$S_g = 60,450 \text{ psi}$$

The stresses calculated above are well within the capabilities of the material selected.

2.2.2.3 Pinion Shaft Bending Stress

The highest stress in the pinion gears occurs in the stub shafts adjacent to the porting holes. It is a bending stress and is subject to complete stress reversals for each revolution of the pinion gear. Using a stress concentration factor of two, the bending stress can be calculated from the following expression:

$$S = \frac{2Mc}{I} \quad (29)$$

where

M = maximum bending moment

c = shaft radius

I = shaft moment of inertia

The stress is calculated to be 14,000 psi and is considerably less than the maximum allowable stress, when using 440C stainless steel, for an infinite endurance life.

2.2.2.4 Output Shaft Torsional Strength

The maximum torsional shear stress in the output shaft is calculated from the following:

$$S_s = \frac{T_m c}{J} \quad (30)$$

where

J = polar moment of inertia

The locations of maximum stress are at the beginning of the spline and in the shaft where the 0.125-inch diameter porting holes are located.

In the spline,

$$S_s = \frac{265 \times 0.24}{\frac{\pi}{32} (0.44^4 - 0.125^4)} = 17,400 \text{ psi}$$

In the shaft,

$$S_s = \frac{265 \times 0.312}{\frac{\pi}{2 \times 32} (0.625^4 - 0.312^4)} = 11,900 \text{ psi}$$

These stresses are also well below the yield point of the gear shaft material.

2.3 SERVOMOTOR TESTS

The initial servomotor tests were conducted using nitrogen gas at storage temperature. After desired performance characteristics were achieved using nitrogen, servomotor performance was established using hydrogen gas at storage temperature. The initial plan was to establish motor performance at cryogenic temperature; however, problems encountered with the servovalve at cryogenic temperature made establishment of the servomotor performance at lower temperatures impossible. Test results indicate that the desired motor performance characteristics were achieved. In Figure 2-10 the actual torque-speed characteristics of the servomotor are shown with the theoretical and required characteristics.

In the following, the servomotor test setup is described and the results of the tests are presented.

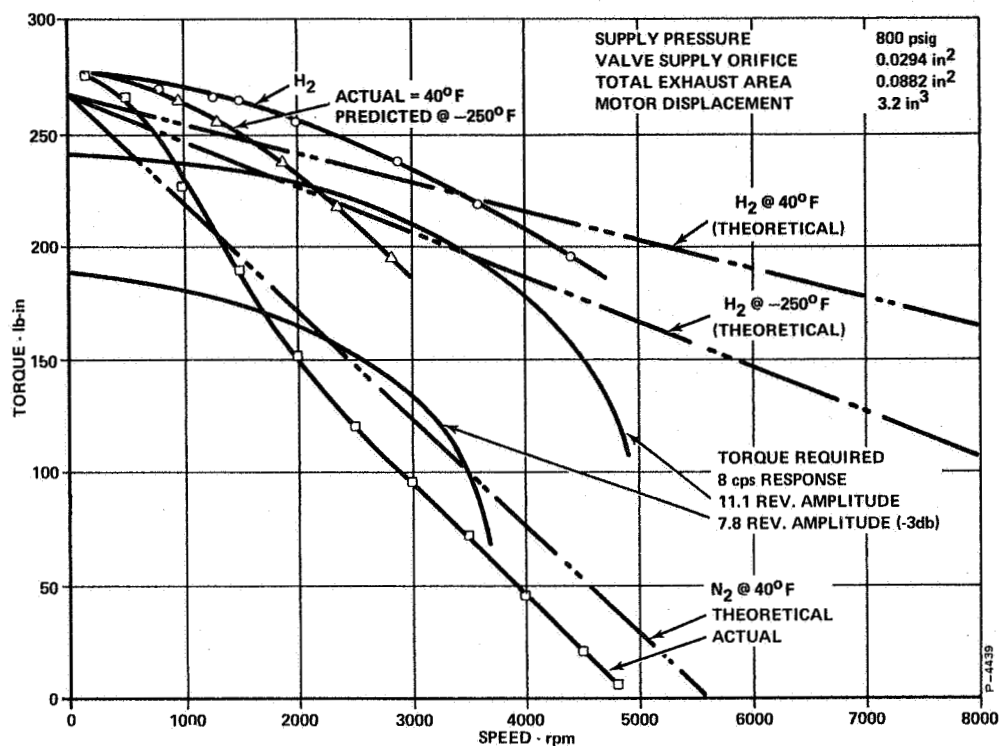


Figure 2-10 - Servomotor Torque-Speed Performance and Requirements

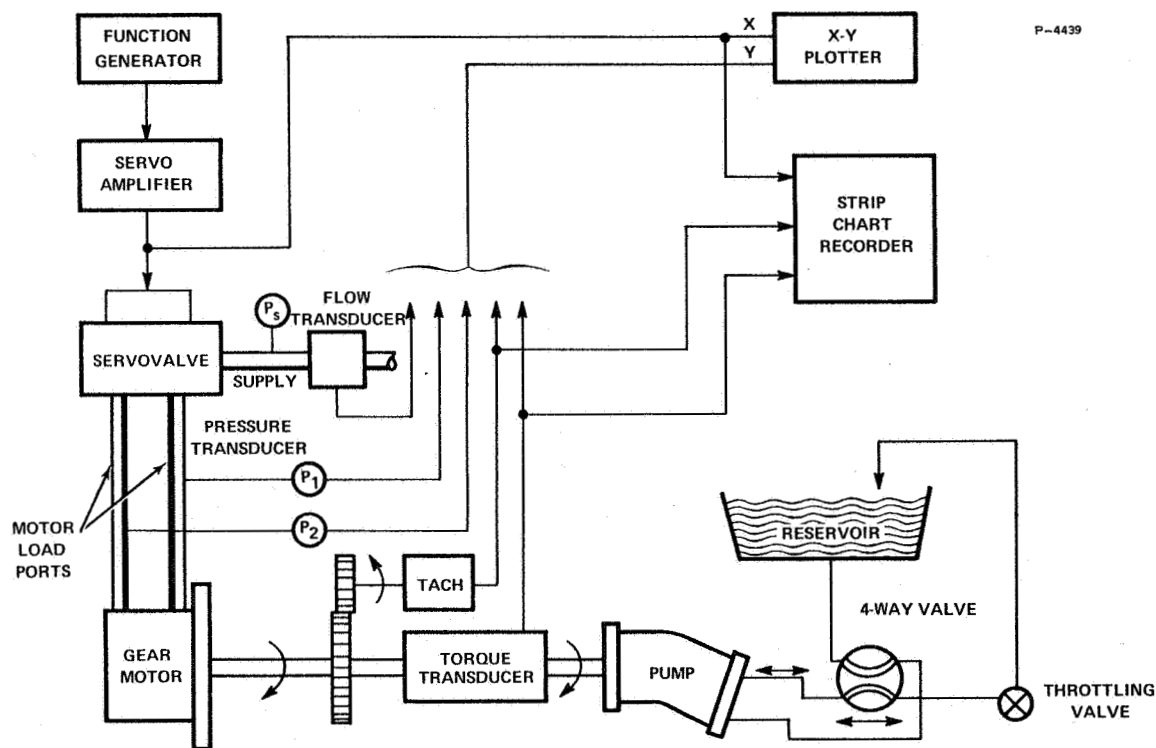


Figure 2-11 - Servomotor Test Setup

2.3.1 Servomotor Test Setup

A schematic of the test setup used to evaluate the performance of the gear type servomotor is shown in Figure 2-11. The servo-valve of the servoactuator is actuated manually through the servoamplifier and actuated electronically by a function generator. When using a function generator, the frequency and amplitude of the input signal may be varied and can be set to have a square, sinusoidal, or triangular wave shape. The supply flow, load port pressures (P_1 and P_2), motor speed, and output torque are measured by electrical transducers. The output of the transducers are recorded either by an X-Y plotter or by a strip chart recorder. The motor load is a hydraulic pump. The load is varied by a throttling valve in the output line of the pump; lead direction is switched by a four-way valve. When conducting tests in which the motor is free running (no-load), the pump is decoupled from the test setup. The output shaft of the torque transducer is locked in place when taking stall torque data.

The same test setup is used during cryogenic tests of the servomotor with the exception that supply flow of gas is routed through a heat exchanger which cools the supply gas. The servomotor is also wrapped in insulation during cryogenic tests. The heat exchanger consists of several coils of tubing immersed in liquid nitrogen.

2.3.2 Motor Tests with Nitrogen

Initial tests of the servomotor were conducted using nitrogen. The servomotor performance was established first in the unported condition, and then the effected porting area on the servomotor speed was established. A porting size was selected and the servomotor performance with the selected porting area was determined. All tests with nitrogen were conducted with gas at storage temperature. The bearings used in the motor, during this phase of testing and during room temperature tests using hydrogen, were standard, off-the-shelf bearings lubricated with light aircraft grease. These bearings were used in this phase of testing because of their much lower cost and shorter delivery schedule.

2.3.2.1 Unported Motor

The motor as initially tested did not have cross-porting. In tests of the unported servomotor, stall torque and free-running speed were determined as functions of torque motor differential current. The data are presented in Figures 2-12 and 2-13. Also determined for a maximum torque motor differential current were torque, differential pressure and gas consumption as functions of speed. From this data, specific fuel consumption and horsepower were calculated. The results are plotted in Figure 2-14.

The no-load frequency response of the unported motor is shown in Figure 2-15.

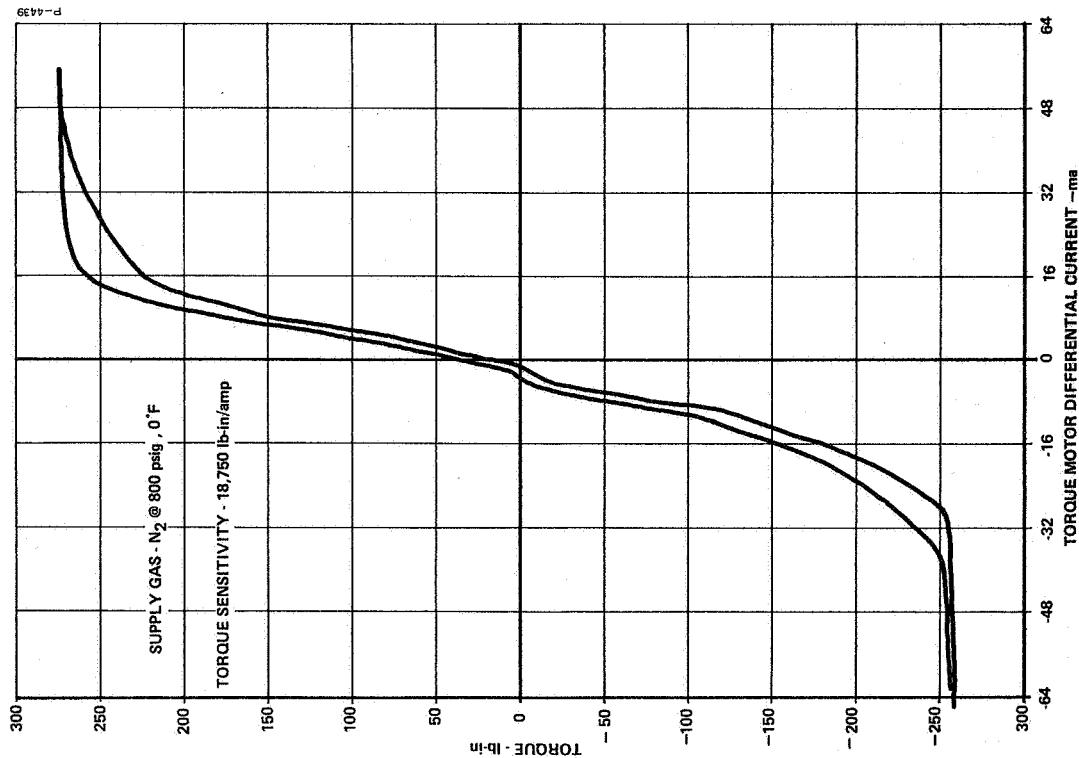


Figure 2-12 - Stall Torque Sensitivity of Unported Servomotor (with Nitrogen)

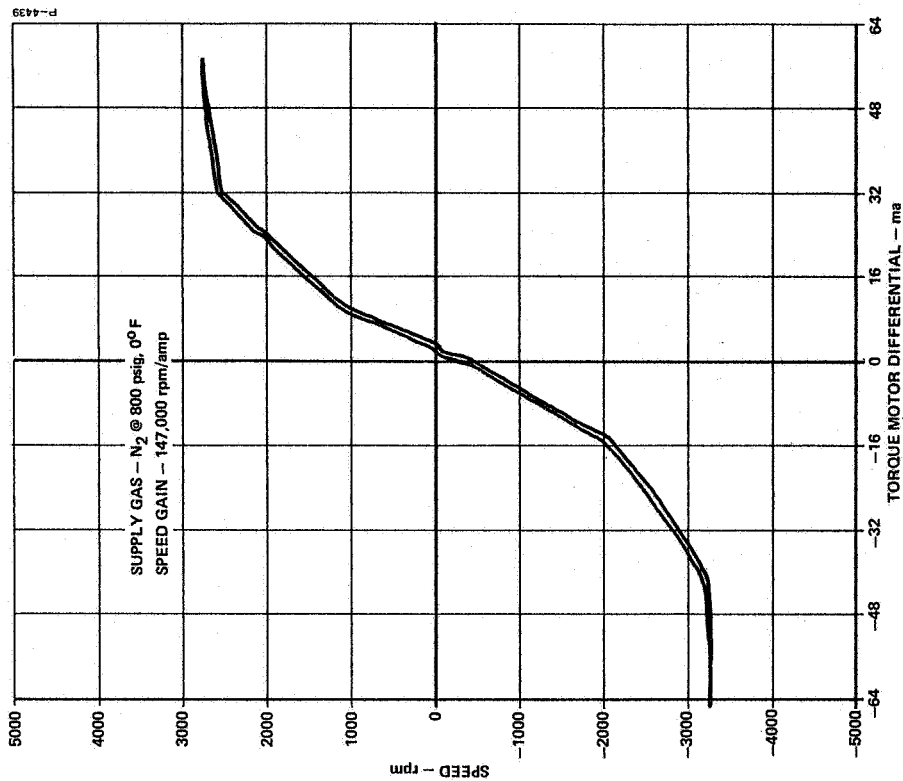


Figure 2-13 - No-Load Speed Sensitivity of Unported Servomotor (with Nitrogen)

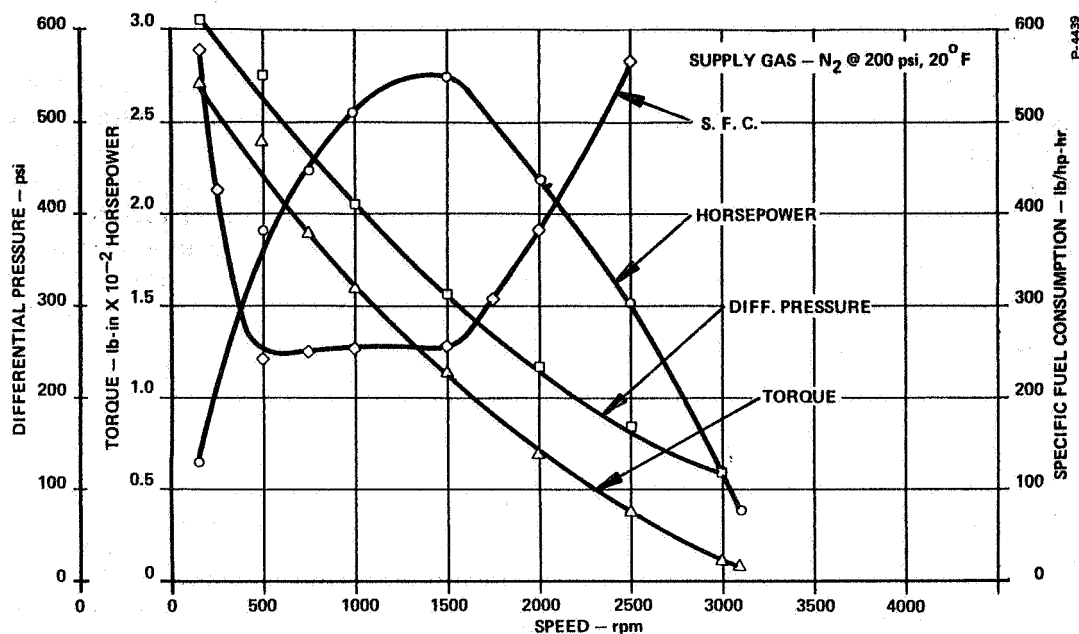


Figure 2-14 - Performance of Unported Servomotor (with Nitrogen)

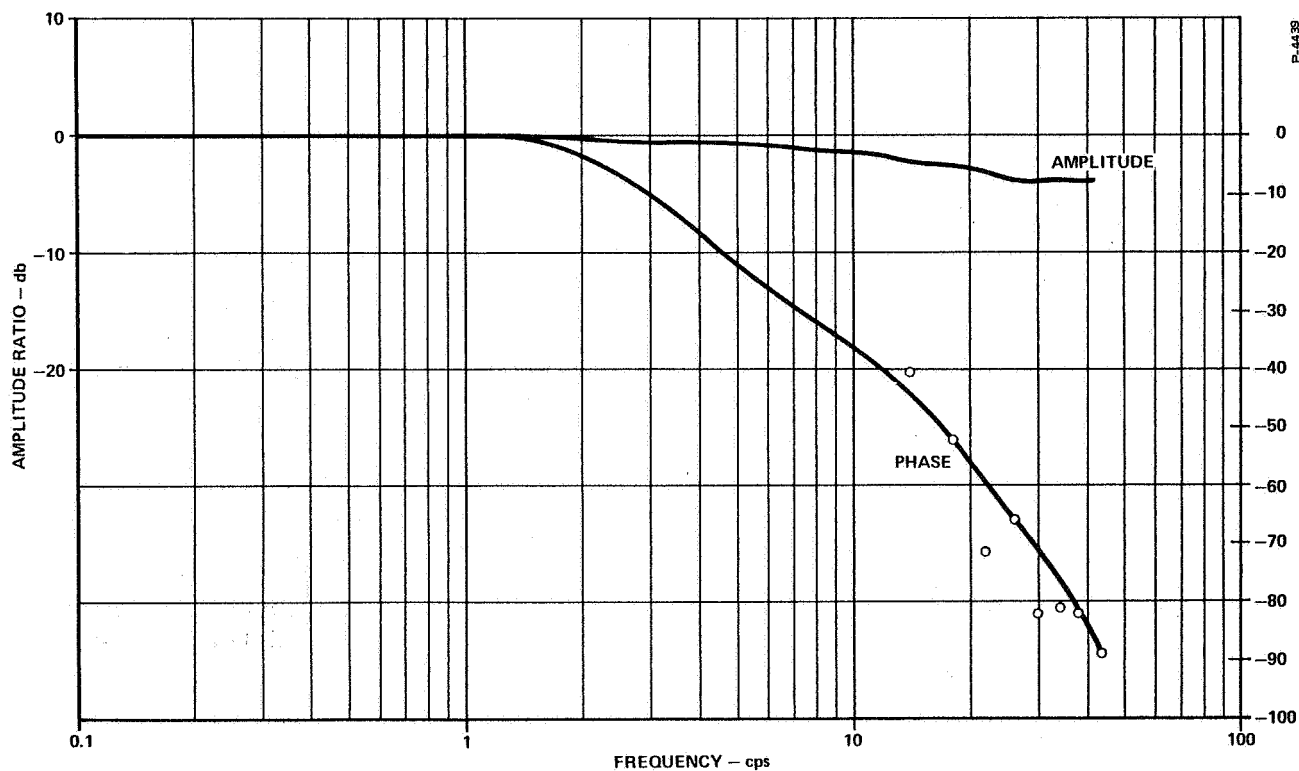


Figure 2-15 - No-Load Frequency Response of Unported Servomotor (with Nitrogen)

2.3.2.2 Cross-Porting Area

To increase the servomotor power and maximum speed, the motor is cross-ported. To determine the proper area of the cross-porting orifice, its area was increased incrementally from an area equal to the maximum servovalve area to an area three times the maximum servovalve area. The motor speed was determined at each increment and the results are shown in Figure 2-16. The desired motor speed was achieved with the cross-port orifice area equal to three times the maximum valve area. This orifice size was incorporated into the motor and used in all subsequent tests.

2.3.2.3 Ported Motor

In tests of the ported motor, stall torque, motor port pressure with motor stalled and free running, and gas consumption with the motor stalled and free running were established as functions of input differential current to the torque motor. The data are presented in Figures 2-17 through 2-21. The motor torque, differential load port pressure, and gas consumption were established as a function of motor speed with the servovalve in the fully open state. The data are presented in Figure 2-22. Horsepower and specific fuel consumption were calculated from the data and are also presented in Figure 2-22.

The frequency response of this servomotor under no-load is shown in Figure 2-23.

2.3.3 Motor Tests with Hydrogen

In tests using hydrogen at its storage temperature, the motor's stall torque, load port pressure, stalled gas consumption and motor speed were determined as functions of servovalve input current. It is possible with hydrogen at its storage temperature of approximately 40°F to achieve very high motor speed that would be damaging to motor bearings; therefore, motor speeds were limited to 5000 rpm. The test results are shown in Figures 2-24 through 2-27. Torque-speed characteristics for maximum servovalve opening were determined up to 4500 rpm. The results of these tests are shown in Figure 2-10.

The off-the-shelf split race bearings used in the motor during the room temperature tests were removed from the motor before cryogenic testing and replaced with the split race bearings made of 440C stainless steel and having a Dupont SP-3 separator to provide necessary bearing lubrication. Tests of motor speed and stall torque as functions of servovalve current were repeated at room temperature and found to be essentially the same as in the previous tests.

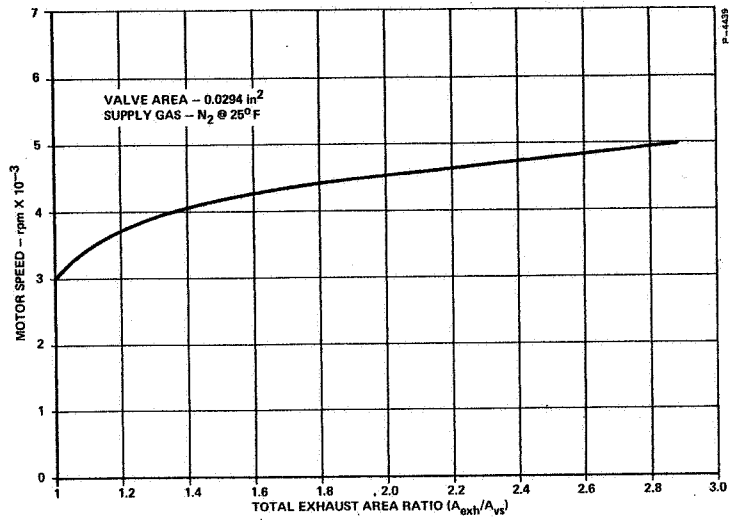


Figure 2-16 - Effect of Cross-Port Orifice Area on Servomotor Speed

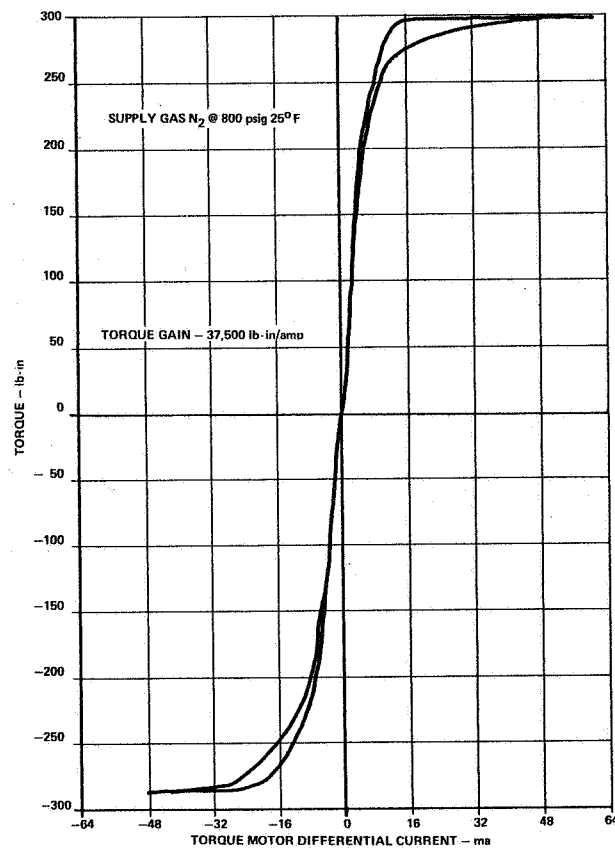


Figure 2-17 - Stall Torque Sensitivity of Ported Servomotor (with Nitrogen)

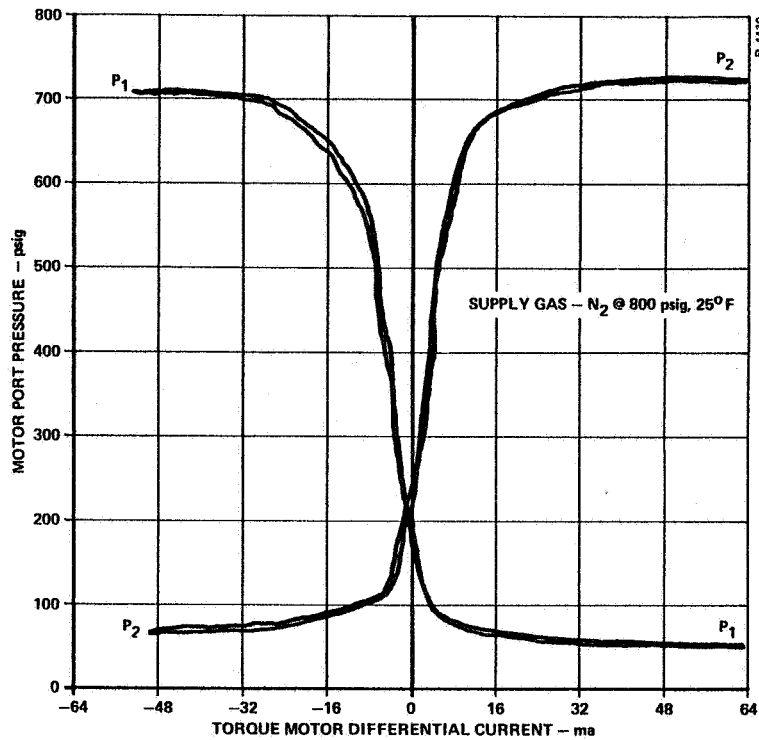


Figure 2-18 - Servomotor Port Pressure at Stall Versus Current (with Nitrogen)

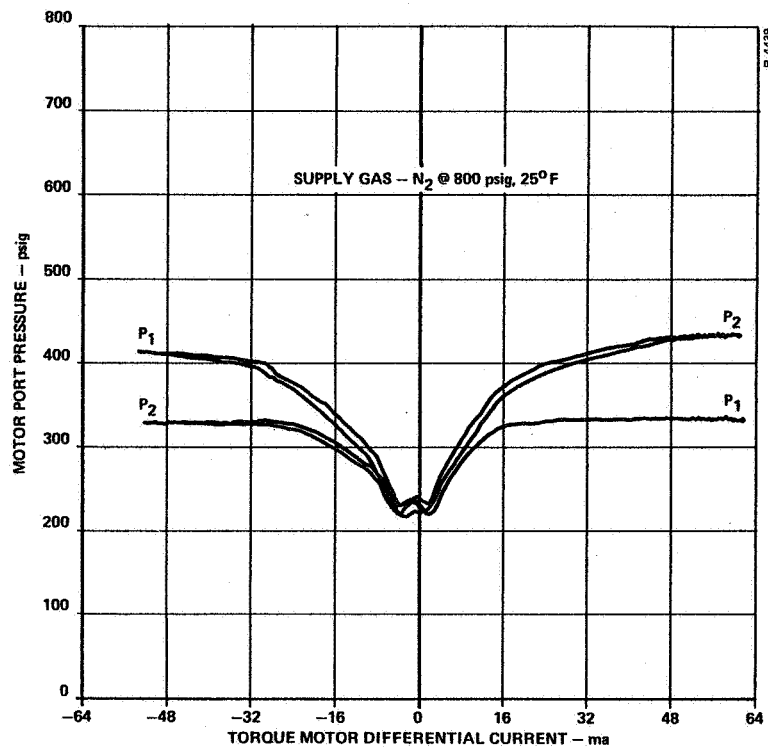


Figure 2-19 - Servomotor Port Pressure, Free Running Versus Current (with Nitrogen)

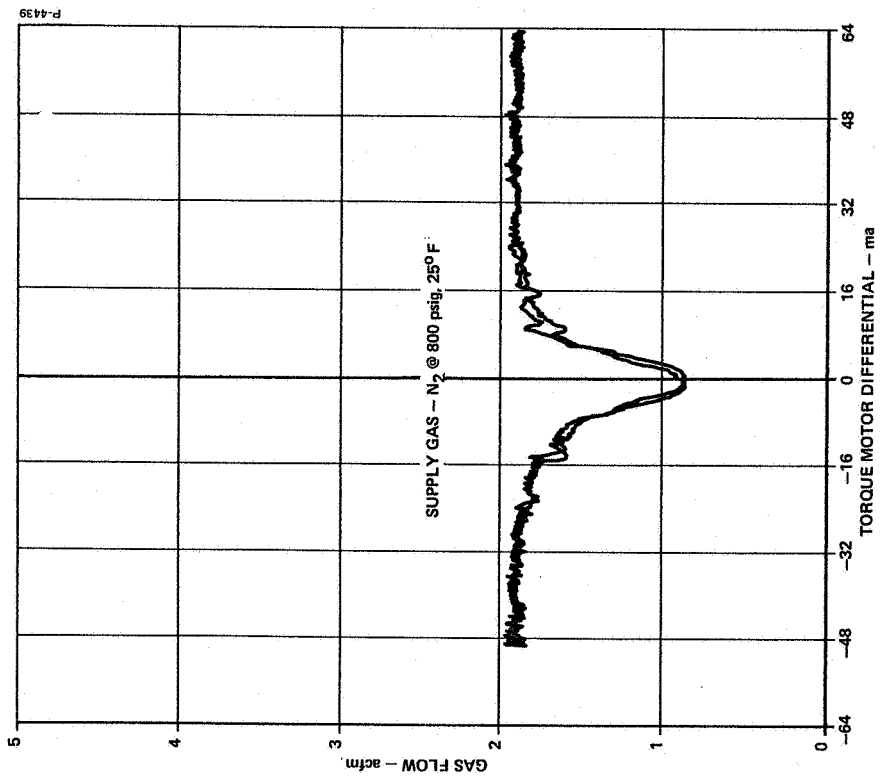


Figure 2-20 - Gas Consumption at Stall Versus Current (with Nitrogen)

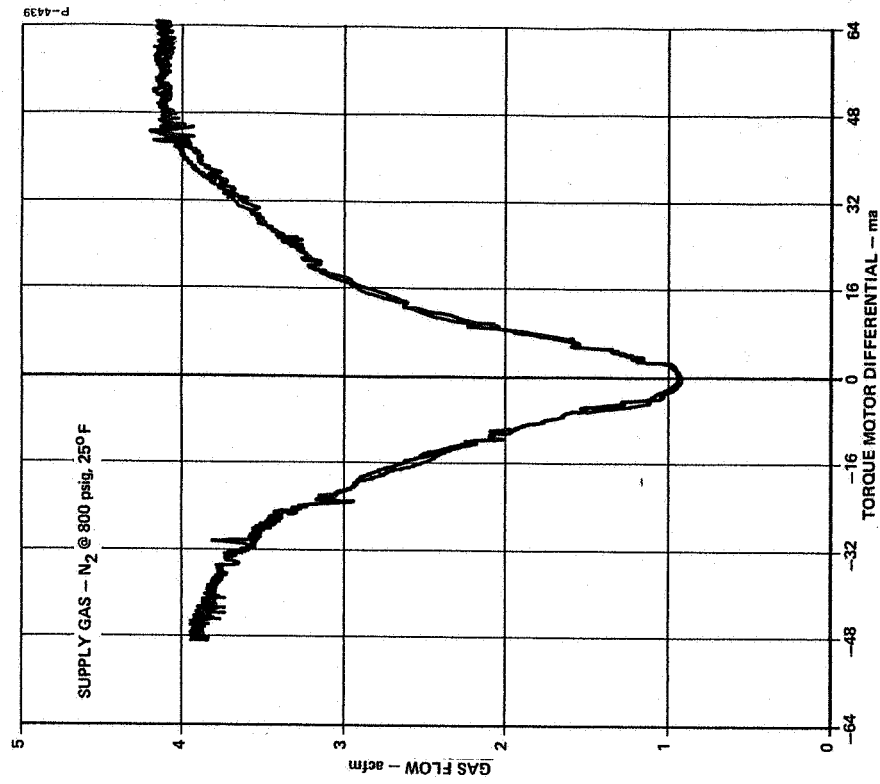


Figure 2-21 - Gas Consumption Free Running, Versus Current (with Nitrogen)

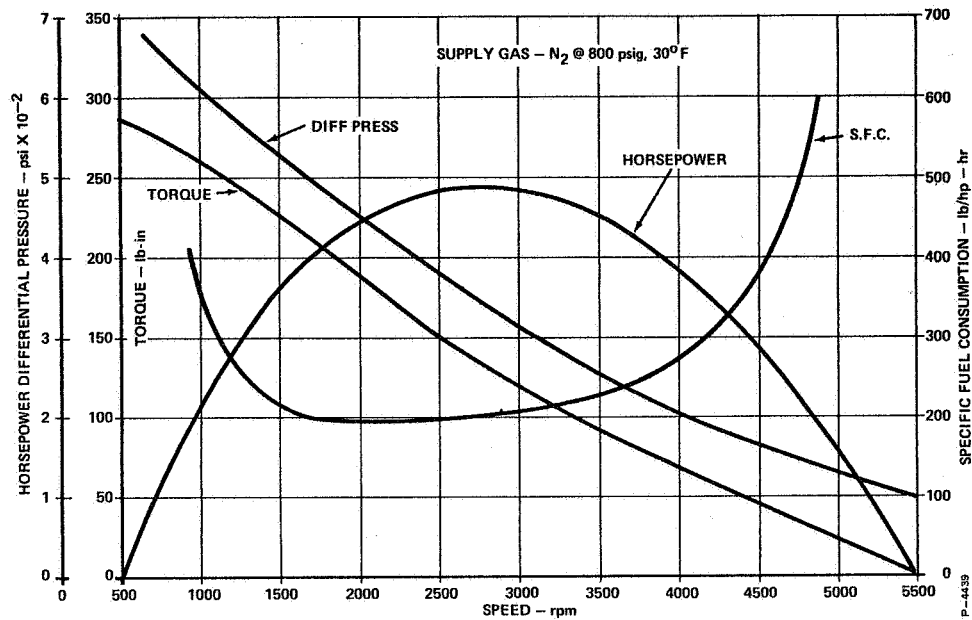


Figure 2-22 - Performance of Ported Servomotor (with Nitrogen)

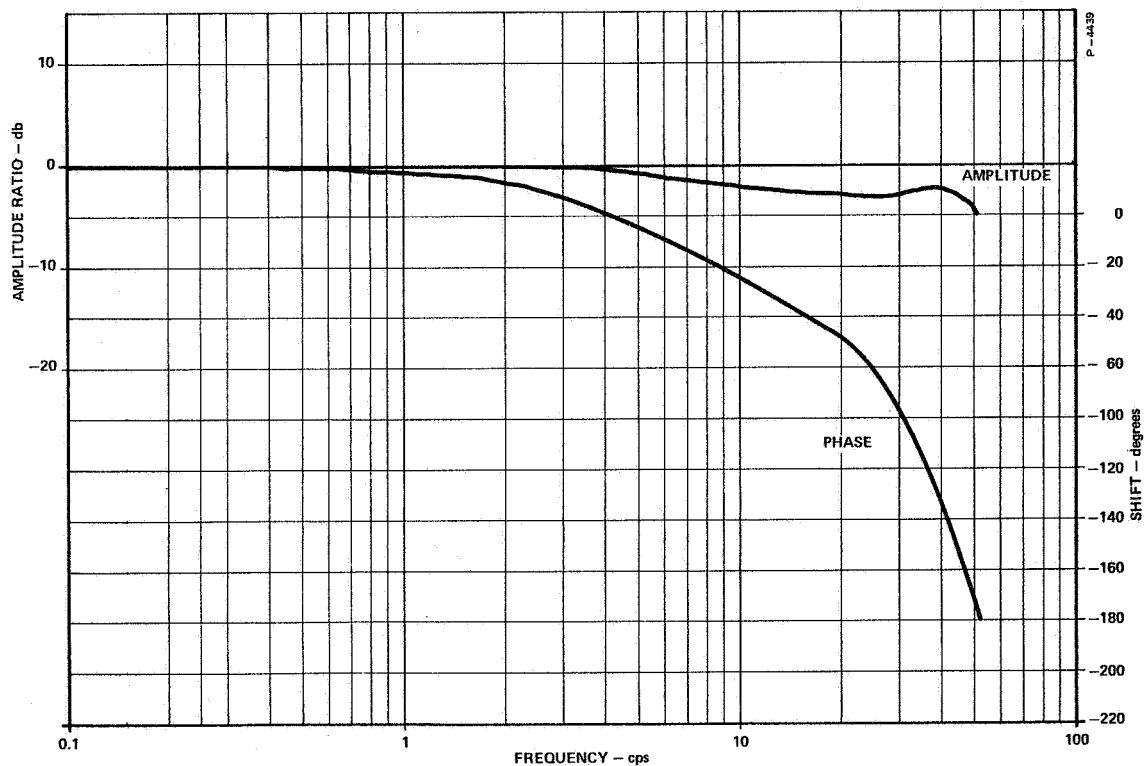


Figure 2-23 - No-Load Frequency Response of Ported Servomotor (with Nitrogen)

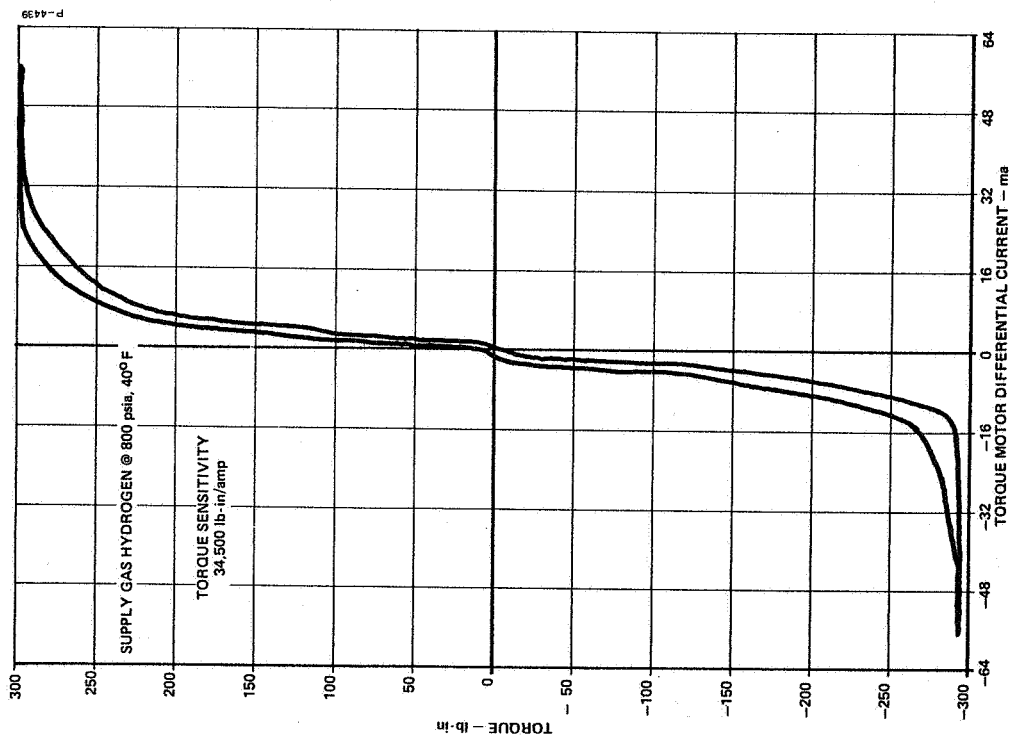


Figure 2-24 - Stall Torque Sensitivity of Ported Servomotor (with Hydrogen)

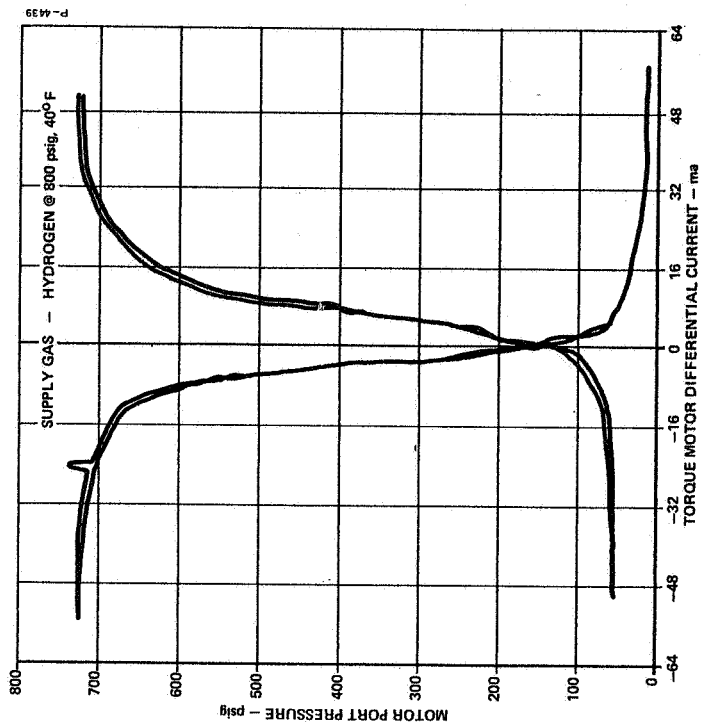


Figure 2-25 - Servomotor Port Pressure at Stall Versus Current (with Hydrogen)

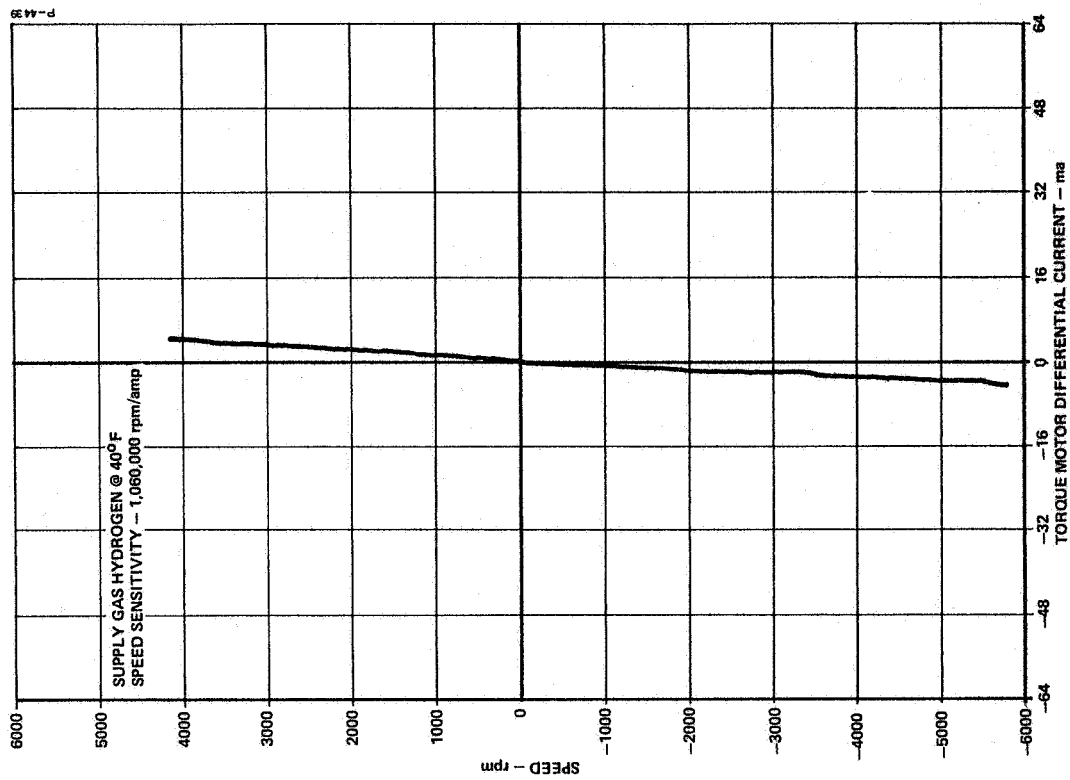


Figure 2-27 - No-Load Speed Sensitivity of Ported Servomotor (with Hydrogen)

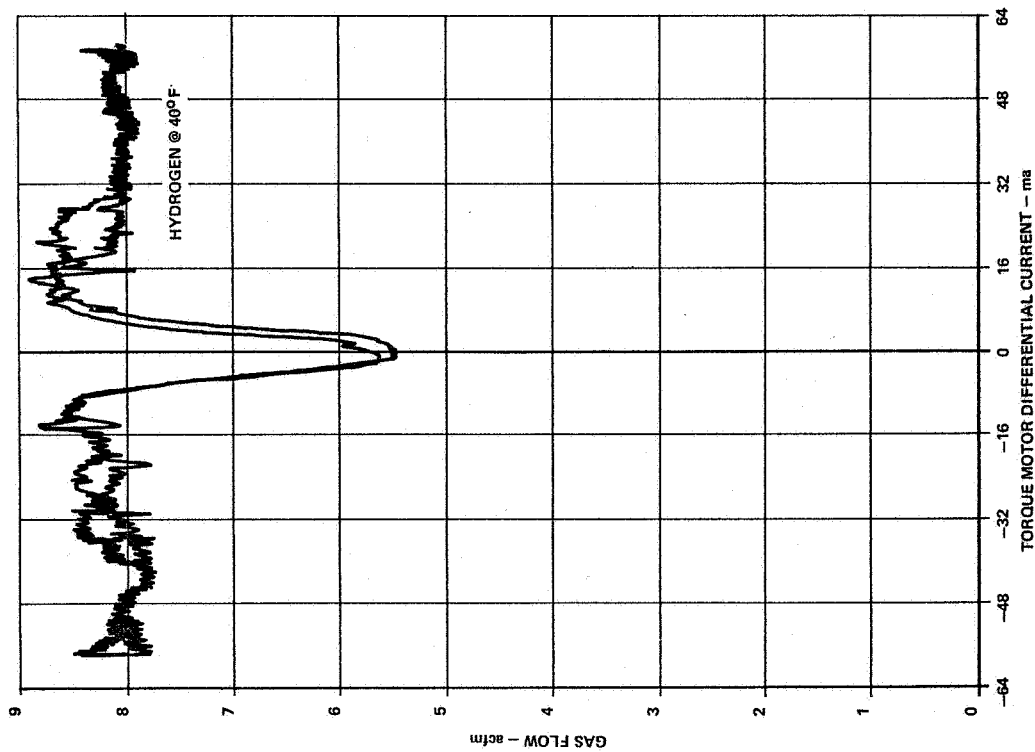


Figure 2-26 - Gas Consumption at Stall (with Hydrogen)

In the cryogenic tests of the motor, control of the motor was lost at temperatures below -150°F and it was not possible to establish motor performance at -250°F . The loss of control was associated with the servovalve which, when stroked from its midposition, would not return. The motor always continued to run during these tests and did not show visible signs of excessive wear even through motor speeds in excess of 7000 rpm were achieved during loss of control.

SECTION 3

SYSTEM EVALUATION

After qualification testing of the J-2 gear motor at room and cryogenic temperatures, the gear motor-servo valve assembly was mounted to the Pneumatic Gimbal Actuator for system evaluation. The NV-B1 Actuator, Serial No. 1, built during the first phase of the program, was used for evaluation of the gear motor in the load simulator test fixture.

Requirements

The Pneumatic Gimbal Actuator must be capable of meeting the following requirements:

System Bandwidth at ± 0.050 -in. Stroke	8 cps
Phase Lag at 1 cps	20 degrees
Peak Amplitude Ratio	1.5 db
Maximum Load	42,000 pounds
Rated Load	23,200 pounds
Made up of:	
Friction Load	7300 pounds
Inertia Load	1400 slugs
Rated Velocity at 23,200 Pounds	1.66 in/sec
Actuator Stiffness - Structural	600,000 lb/in
Rated Servo Current	40-50 ma
Fluid Medium	
Room temperature Gaseous Nitrogen	800 psig
-250°F Gaseous Hydrogen	800 psig

3.1 TEST FIXTURE

A walking beam simulator fixture, used to evaluate the NV-B1 actuator, provides the inertia load of 1400 slugs and a friction load of 7300 pounds. The structure of the simulator fixture was designed to have a resonant frequency of 9.2 cps.

To record actuator output force, a strain gage was mounted on the rod end attaching clevis. A similar strain gage was mounted on the connecting rod between the walking beam and the brake arm. For recording inertia travel, a rotary variable differential transducer was attached to the beam supporting shaft. The position indicator section of the

actuator feedback potentiometer was used to record actuator position. Friction load was provided by regulated hydraulic pressure to the non-servo brake.

A hydraulic load cylinder was solid mounted in an identical position to the actuator on the opposite side of the beam supporting shaft to provide the rated load of 23,200 pounds. This cylinder was double-acting with interconnecting plumbing so that a relief valve setting would produce the same resistive load in each direction. The cylinder could also be connected to a hydraulic supply to load the actuator in either direction to obtain actuator stiffness.

3.1.1 Load Fixture Instrumentation

The schematic of the load fixture, its associated instrumentation, and its placement is shown in Figure 3-1. The load fixture was instrumented to provide load inertia position, load friction force, and actuator force. The load friction force was determined by measuring the elongation of its connecting rod with a strain gage and calibrating this with respect to the force generated at the actuator attaching point. The load inertia position was determined by measuring the angular displacement of the beam support shaft with respect to the beam supporting structure by means of a rotary position transducer. The constant force generated by the hydraulic piston was measured at the actuator attaching point with a strain gage.

The load friction force, load inertia position, and actuator force signals were fed into a Sanborn carrier and amplifier system and converted to dc signals for recording purposes.

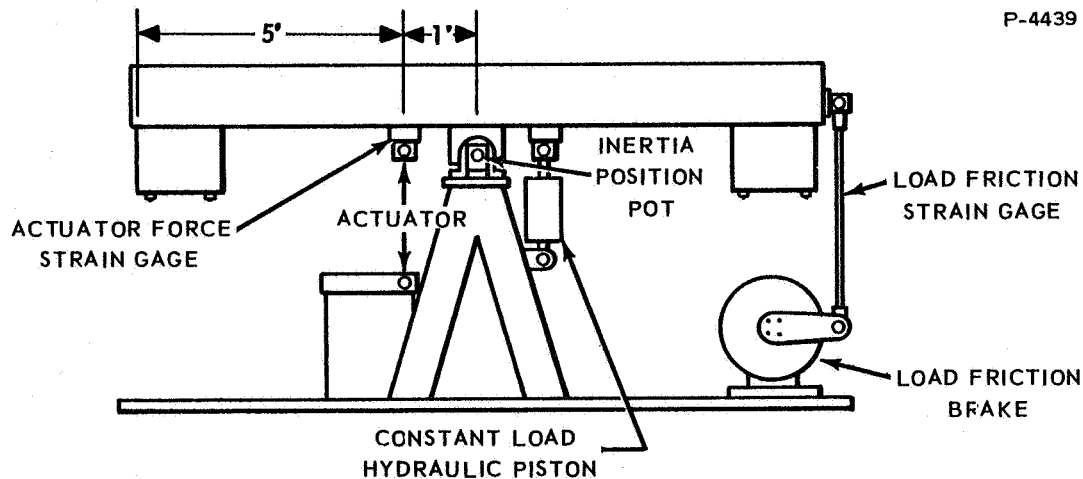


Figure 3-1 - Load Fixture and Instrumentation Schematic

3.1.2 Pneumatic System

The pneumatic system schematic for both room temperature and low temperature testing is shown in Figure 3-2.

The room temperature tests employed nitrogen at a supply pressure of 800 psig. All low temperature tests were conducted with hydrogen at a supply pressure of 800 psig. To facilitate rapid shutdown of the control system servo pressure, should an emergency arise, and to facilitate purging of the control system with nitrogen prior to running with hydrogen, a pair of solenoid valves was installed upstream of the actuator. Both hydrogen and nitrogen supply pressures were remotely adjustable by means of a dome regulator. In addition, the nitrogen supply pressure was made adjustable with a loading valve. Gas flow was measured with a Cox GM-8 turbine flowmeter.

Low temperature hydrogen gas was obtained by passing ambient temperature hydrogen gas through a liquid nitrogen cooled heat exchanger. The temperature of the gas was controlled by regulating the liquid nitrogen coverage of the tubing in the heat exchanger.

3.1.3 Control System Wiring and Instrumentation

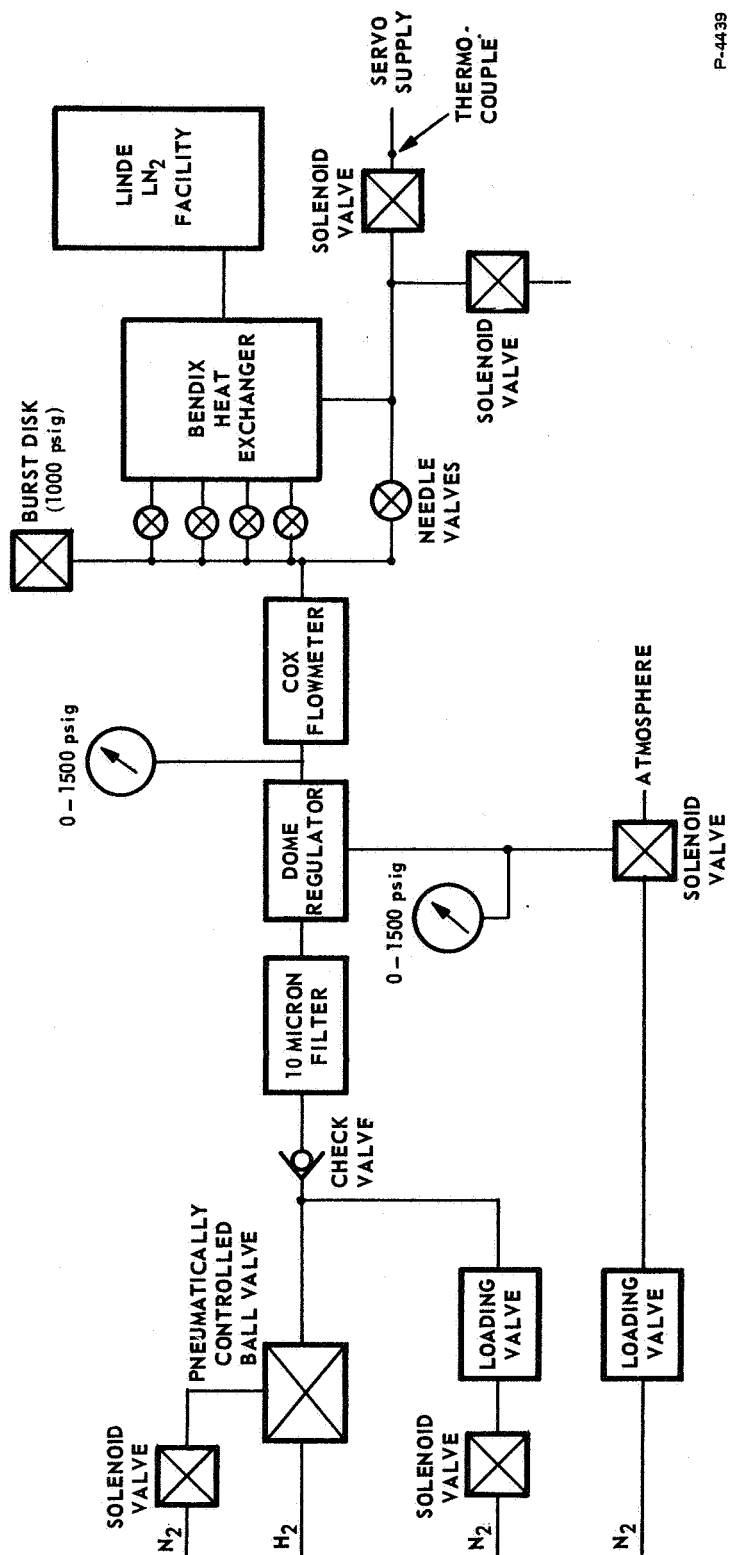
The control system and instrumentation wiring diagram is shown in Figure 3-3. The control system was instrumented to provide, for recording purposes, torque motor current, actuator dynamic forcing function, and actuator position. Torque motor current was determined by measuring the voltage across a 10-ohm resistor in series with the torque motor coils. Actuator position was determined by measuring the voltage from the spare element of the actuator dual-element potentiometer.

The torque motor of the servoactuator was driven by a dc servoamplifier consisting of the amplifier proper and a 15-vdc power supply. The power supply is used as a power source for the amplifier and the actuator dual-element potentiometer.

3.1.4 DC Servoamplifier

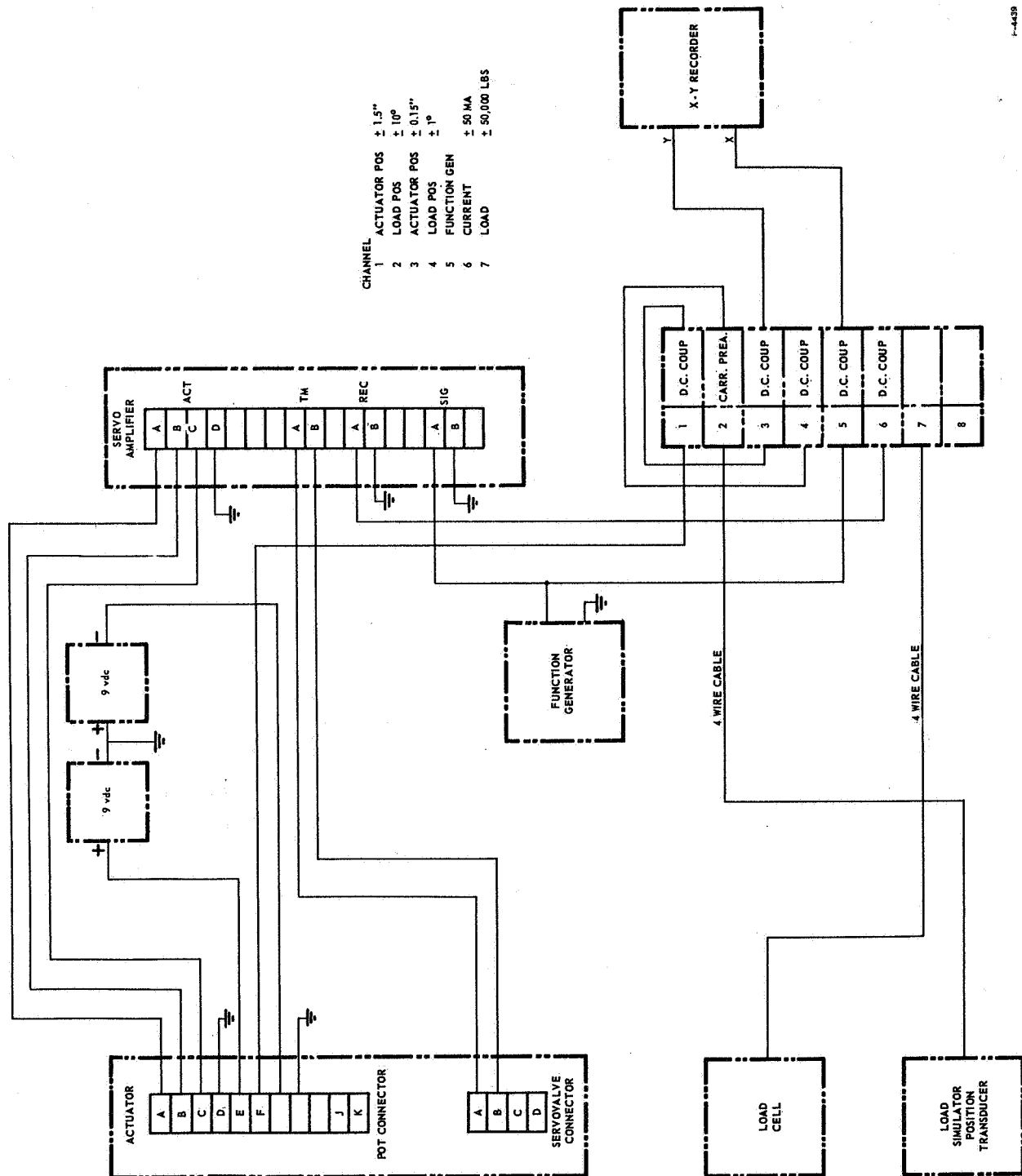
Several amplifier compensation circuits were used during testing to establish the best means of compensating the actuator. Initially, a rate feedback compensation circuit and lead-lag circuit were used to obtain system performance. Figure 3-4 is a block diagram of this configuration. The feedback voltage signal is electronically differentiated by the amplifier to form the rate signal, which is then summed with the error voltage between the feedback and the demand signal. The summed signal is sent through a lead-lag circuit and a current driver stage to drive the servovalve torque motor. Although this circuit is basically feasible, it did not completely compensate for the load resonance peak, and a 10-db peak in the frequency response occurred.

To achieve better compensation of the actuator, a load pressure feedback circuit was also used. The block diagram of the amplifier for this configuration is shown in Figure 3-5. A pressure transducer



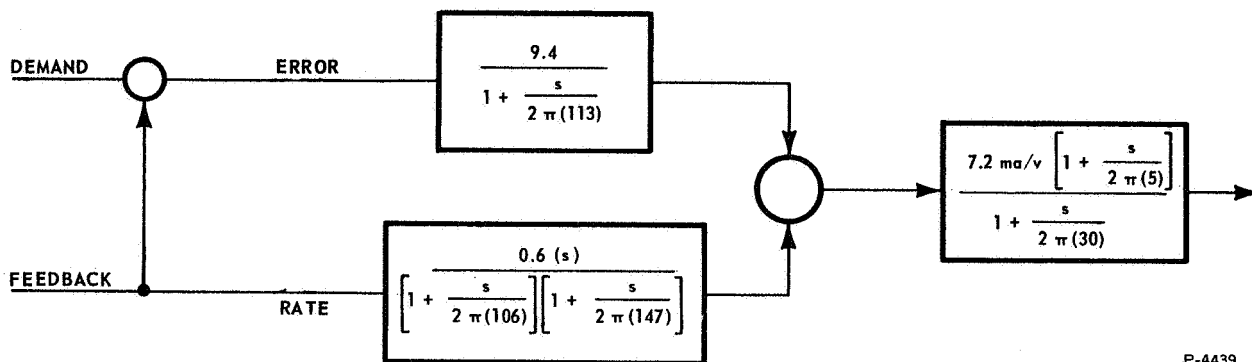
P-4439

Figure 3-2 - Pneumatic System Schematic



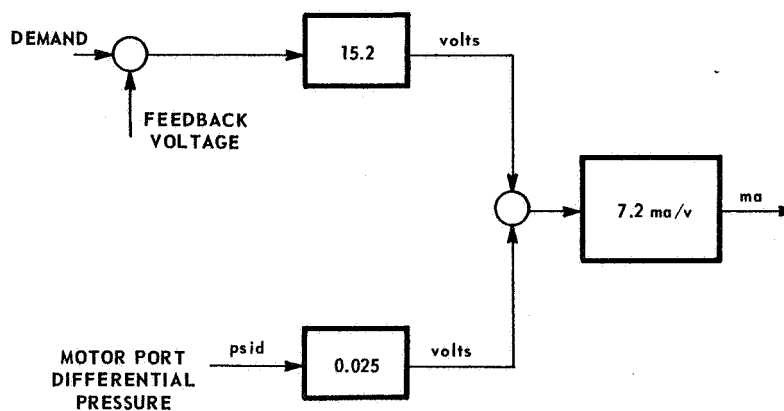
1-4439

Figure 3-3 - J-2 Instrumentation Diagram



P-4439

Figure 3-4 - J-2 Servoamplifier Block Diagram



P-4439

Figure 3-5 - Pressure Feedback Block Diagram

was installed across the motor ports between the servovalve and the motor. This signal would be the same as a true pressure feedback signal within the servovalve, had the valve been so designed. This transduced load-pressure feedback adequately compensated the actuator, causing the frequency response of the load to be flat. Further testing using dynamic pressure feedback was not tried because the actuator ball nut failed.

3.2 OPEN-LOOP AND CLOSED-LOOP PERFORMANCE

Both open-loop and closed-loop tests were conducted on the Pneumatic Gimbal Actuator with the gear motor installed. The open-loop tests were conducted to obtain information necessary to complete the servoamplifier circuit and insure stable closed-loop operation of the actuator.

The following performance parameters were monitored in closed-loop operation:

- Frequency Response
- Transient Response
- Actuator Linearity
- Actuator Hysteresis

The above tests were conducted with a room temperature nitrogen supply at a pressure of 800 psig. The frequency response and the transient response tests were conducted with a friction load of 7300 pounds and with no-load friction.

3.2.1 Rate Compensation

The phase lag and amplitude ratio at room temperature with rate feedback compensation are plotted in Figure 3-6 for no-load friction and in Figure 3-7 for a friction load of 7300 pounds. The room temperature linearity curve for the J-2 actuator with a pneumatic gear motor is shown in Figure 3-8, while Figure 3-9 is the hysteresis curve for the actuator. The room temperature transient response with no-load friction and for a friction load of 7300 pounds is shown in Figure 3-10. The closed-loop performance data, from which Figures 3-6 and 3-7 were obtained, are shown in Figures 3-11 through 3-14.

3.2.2 Pressure Feedback Compensation

Amplitude ratio for room-temperature, no-load friction is plotted in Figure 3-15, and transient response is plotted in Figure 3-16. Linearity and resolution are shown in Figures 3-17 and 3-18.

3.3 CONCLUSIONS

The J-2 pneumatic actuator performance has been upgraded by replacing the existing vane servomotor with a gear servomotor. The 8-cps bandwidth requirement is exceeded as the -3-db point occurs at a frequency greater

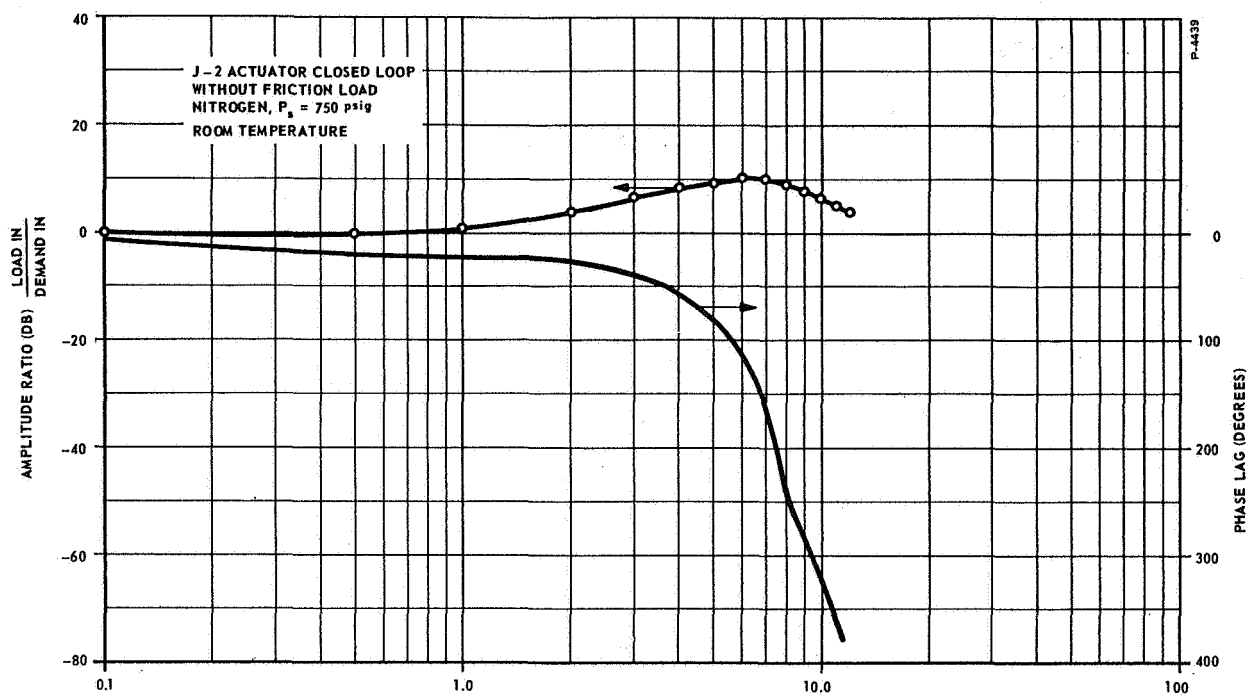


Figure 3-6 - J-2 Actuator Closed Loop Response (Without Friction Load)

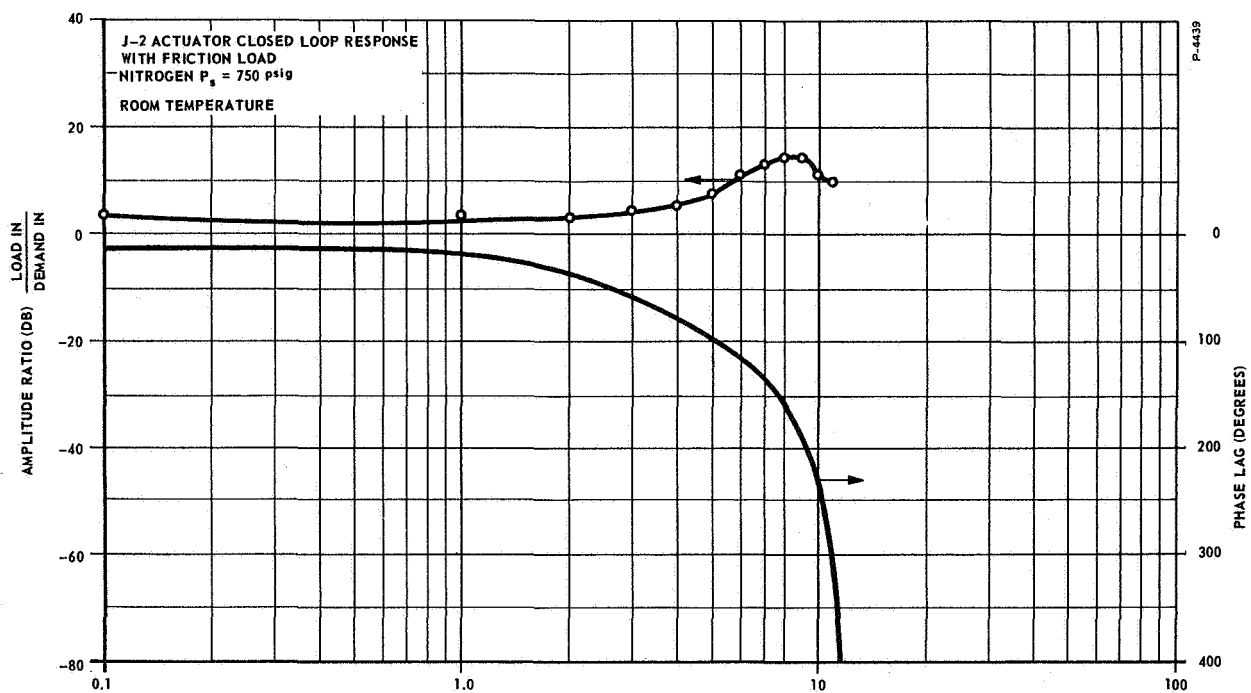


Figure 3-7 - J-2 Actuator Closed Loop Response (With Friction Load)

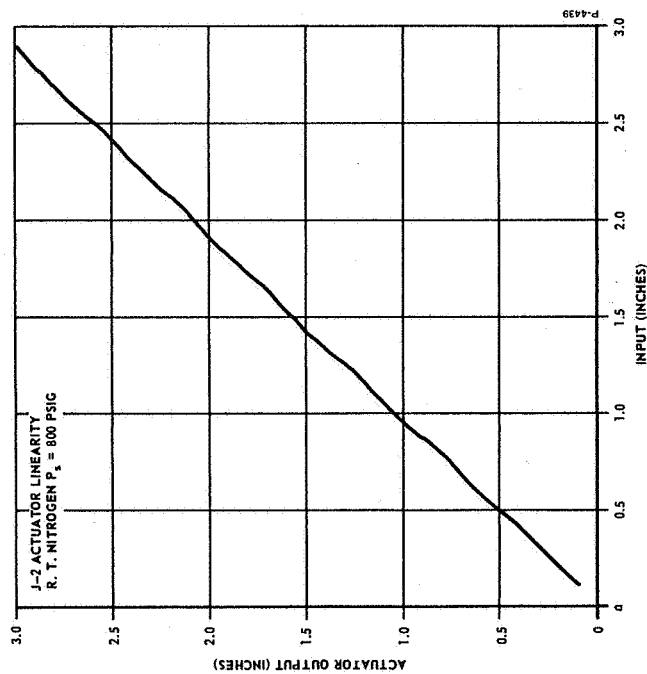


Figure 3-8 - J-2 Actuator Linearity

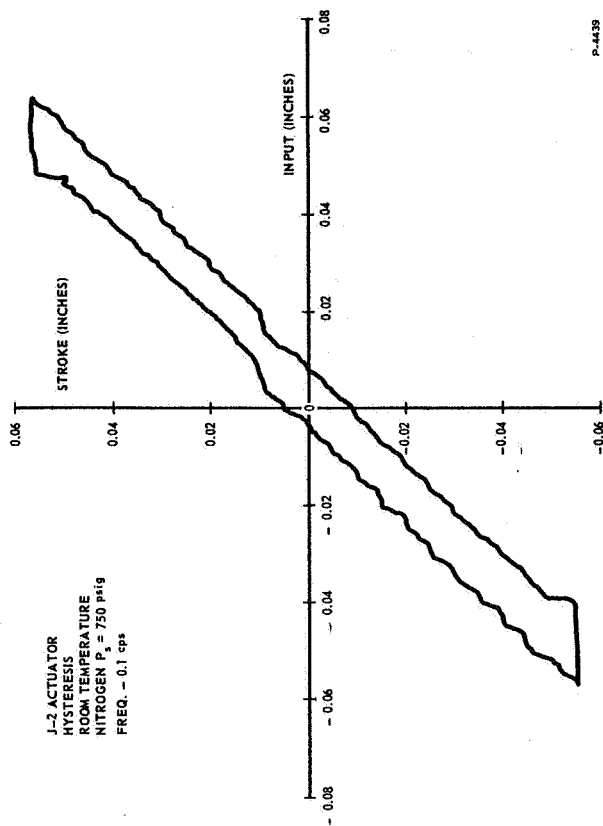


Figure 3-9 - J-2 Actuator Hysteresis

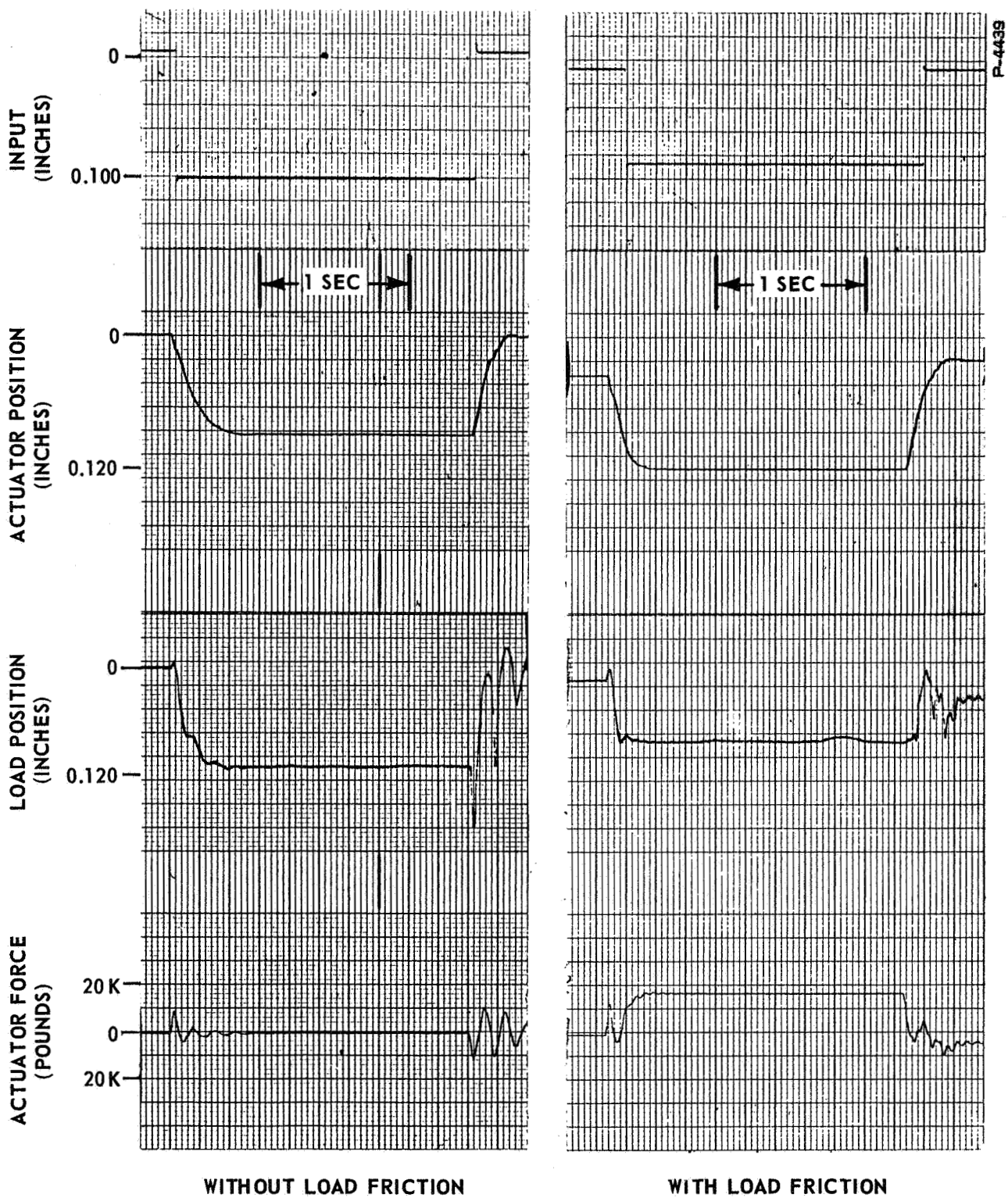


Figure 3-10 - Transient Response Without and With Load Function

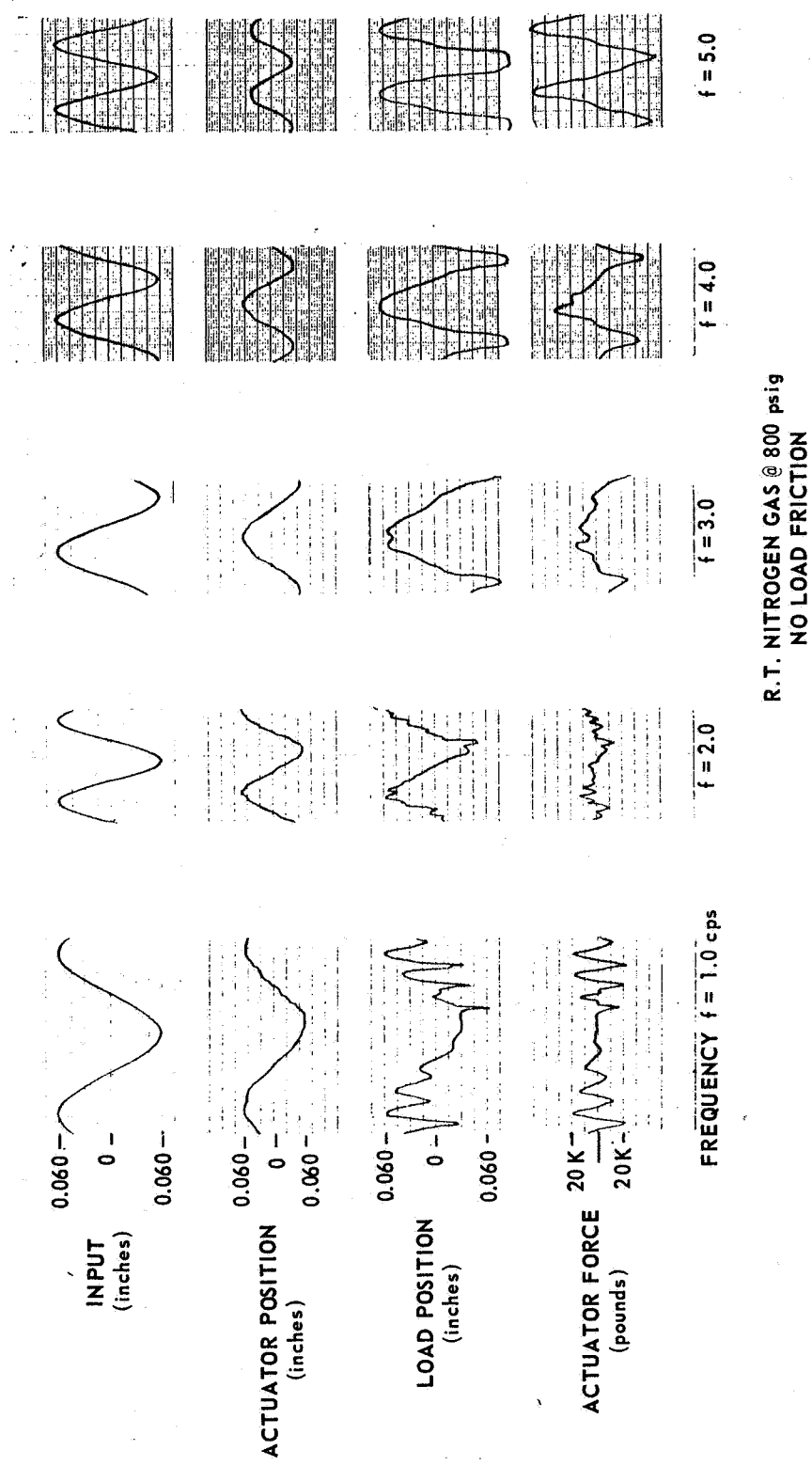
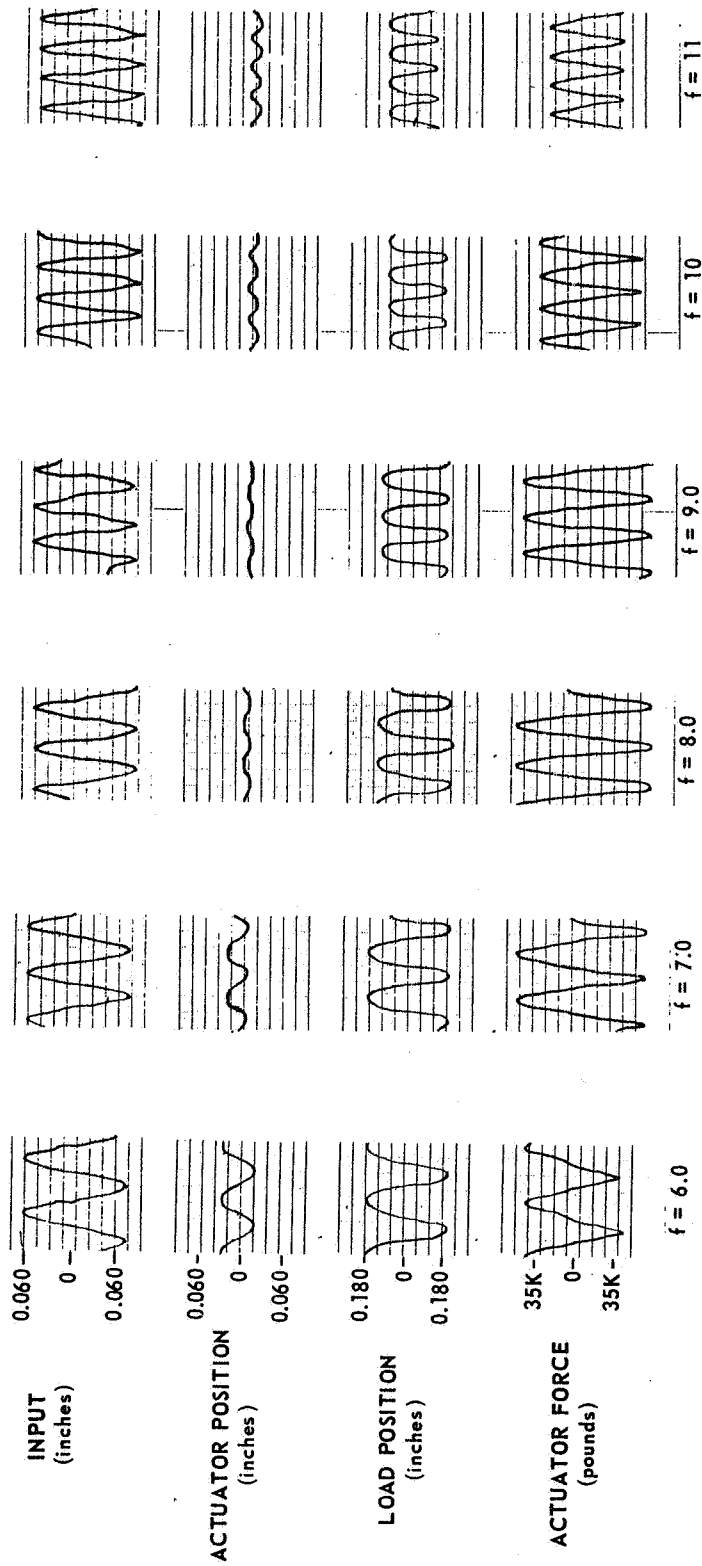
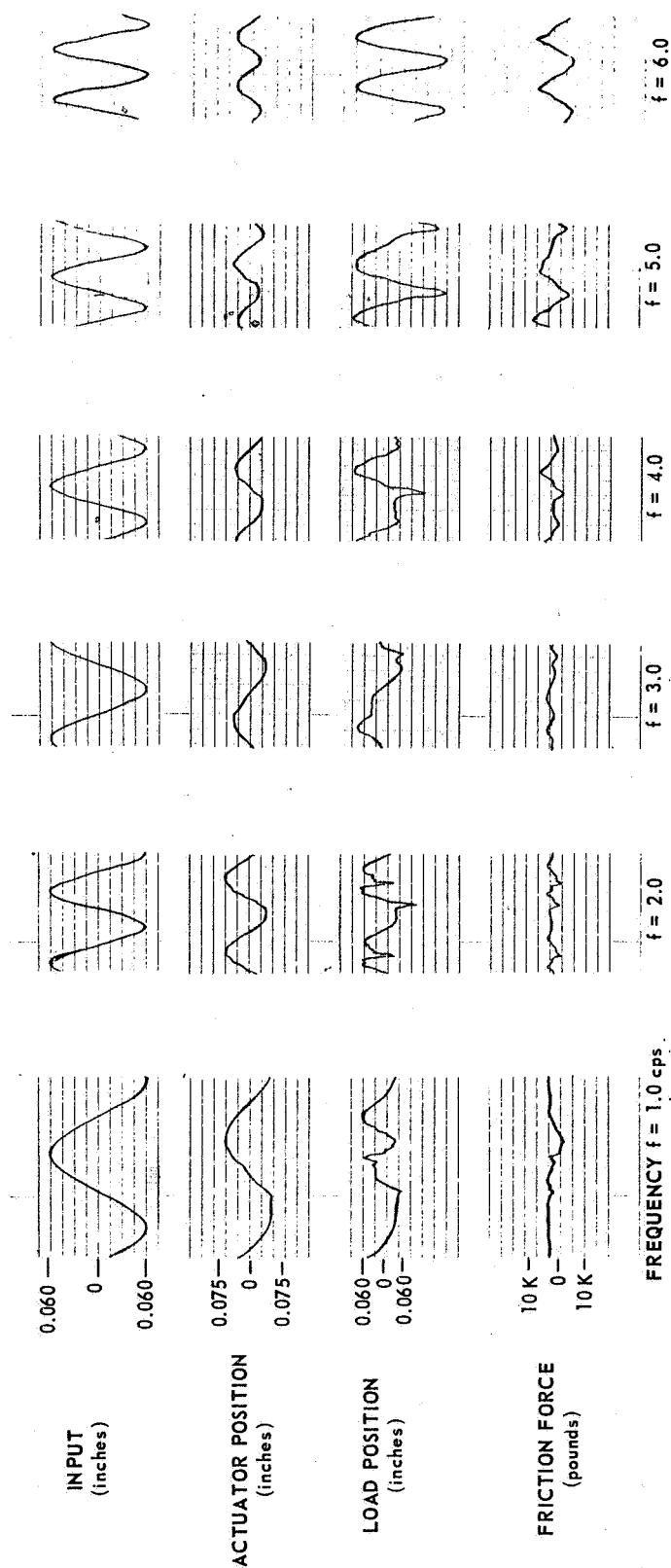


Figure 3-11 - Actuator Closed-Loop Frequency Response
($f = 1$ cps to $f = 5$ cps; Actuator Position = 0.060 in.)



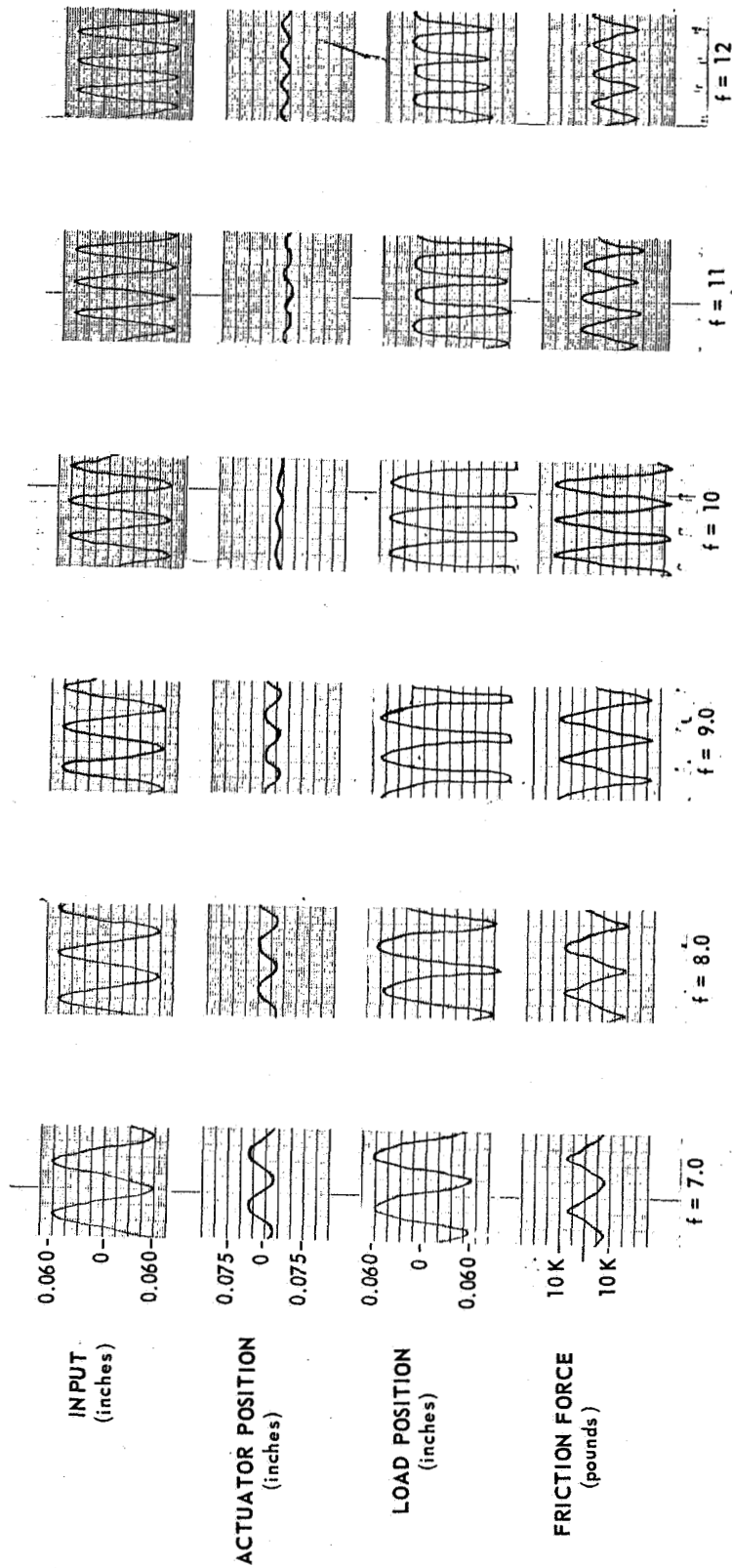
R.T. NITROGEN GAS @ 800 psig
NO LOAD FRICTION

Figure 3-12 - Actuator Closed-Loop Frequency Response
($f = 6$ cps to $f = 11$ cps; Actuator Position = 0.060 in.)



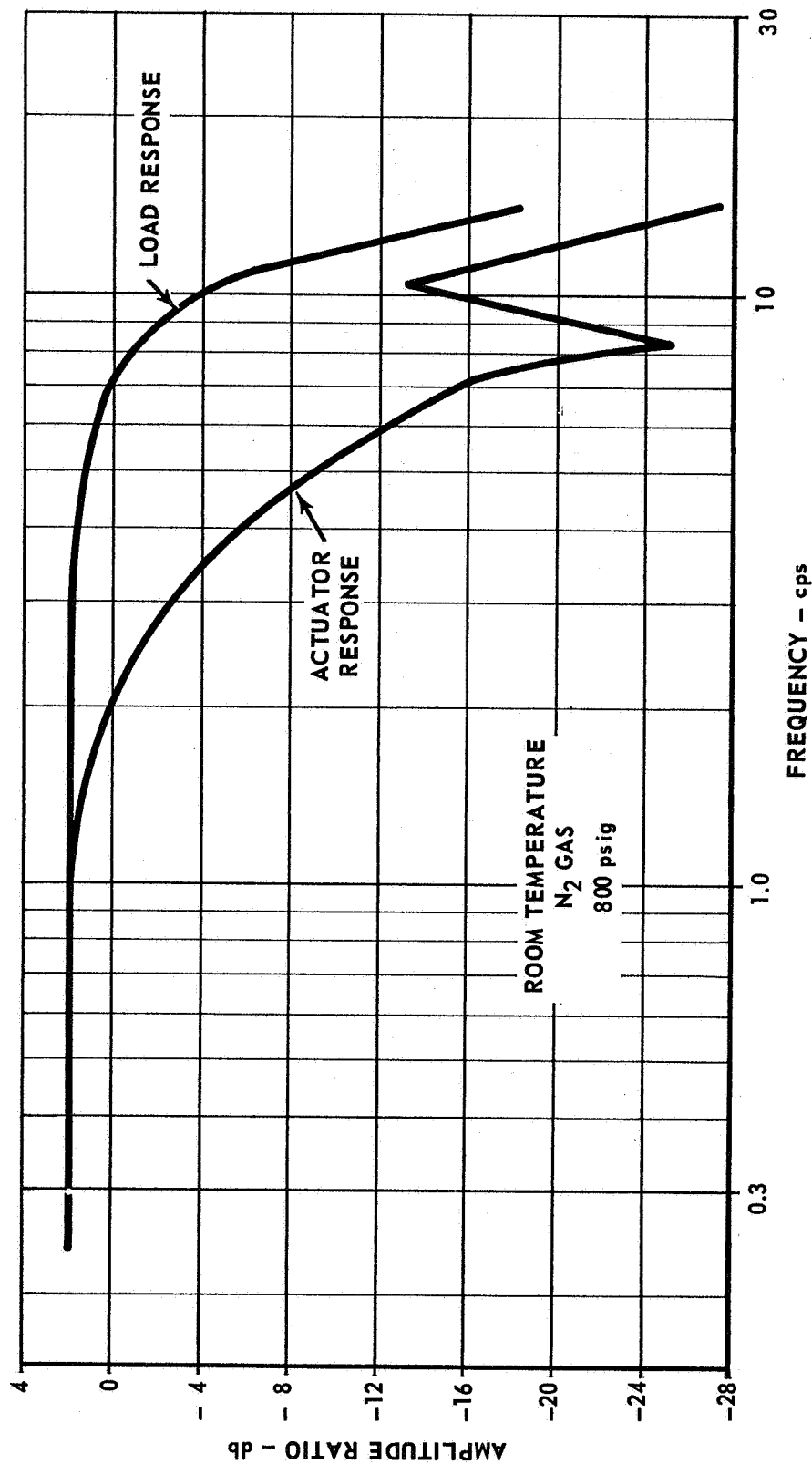
R. T. NITROGEN GAS @ 800 PSIG
WITH LOAD FRICTION

Figure 3-13 - Actuator Closed-Loop Frequency Response
($f = 1$ cps to $f = 6$ cps; Actuator Position = 0.075 in.)



R.T. NITROGEN GAS @ 800 psig
WITH LOAD FRICTION

Figure 3-14 - Actuator Closed-Loop Frequency Response
($f = 7$ cps to $f = 12$ cps; Actuator Position = 0.075 in.)



P-4439

Figure 3-15 - Frequency Response with Pressure Feedback, No-Load Friction

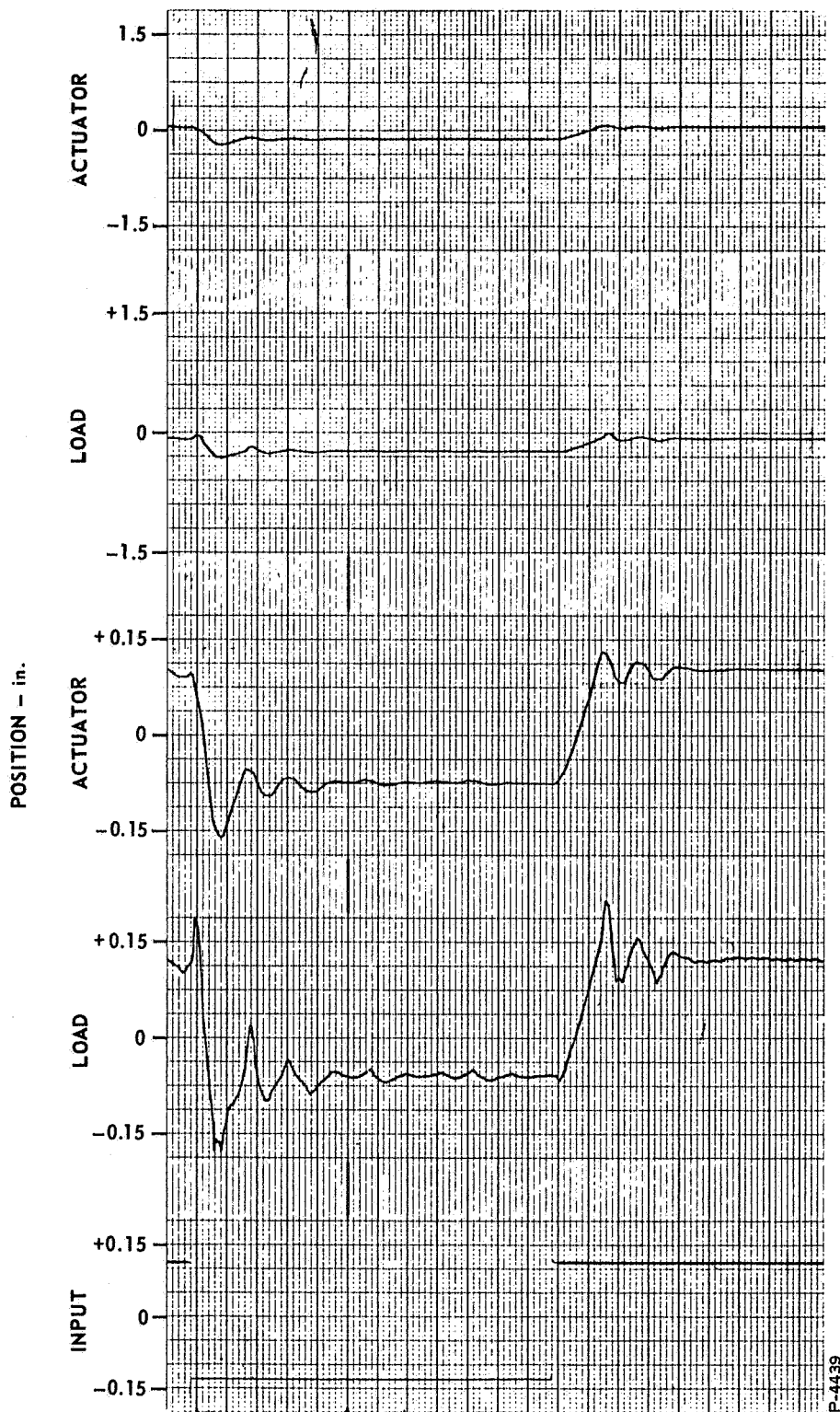


Figure 3-16 - Transient Response with Pressure Feedback

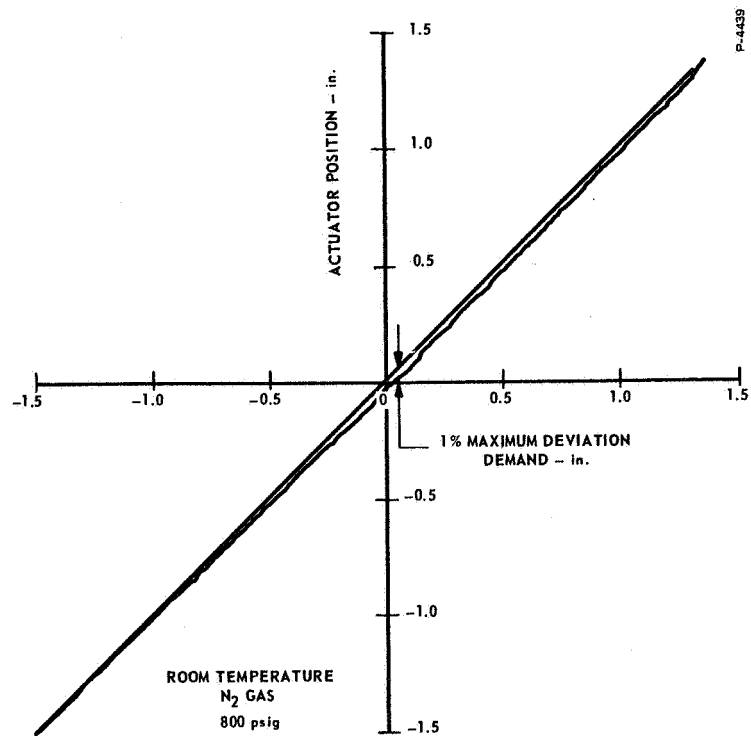


Figure 3-17 - Actuator Linearity with Pressure Feedback

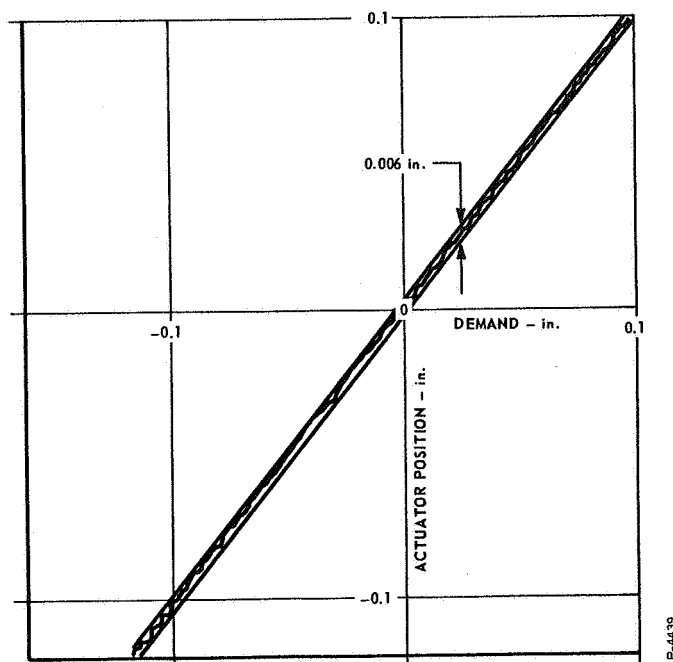


Figure 3-18 - Actuator Resolution with Pressure Feedback

than 10 cps, both with no-load friction and with a friction load of 7300 pounds, with rate compensation. The phase lag at 1 cps is less than 20 degrees. The J-2 actuator with the vane servomotor had a phase lag of 28 degrees at 1.0 cps and a bandwidth of 3.5 cps. Deadband in the actuator has been reduced by the elimination of the vane friction losses which are characteristic of a vane servomotor. The transient response was well within reason with respect to the rise time, overshoot, and settling time. Pressure feedback compensation adequately damps the load resonance, and a system with dynamic pressure feedback built into the servovalve would perform as well as a piston-cylinder hydraulic system. Actuator failure, caused by the higher performance gear motor, stopped testing while using hydrogen at -250°F . However, the results shown in the previous sections establish adequate performance of a pneumatic gimbal actuator of this type, and a new actuator, designed to flightweight standards and incorporating the technology developed in this program, will easily perform the engine gimbaling function.

APPENDIX A

EFFECT OF THERMAL CYCLING AND CRYOGENIC TEMPERATURES
ON ADHESIVE SHEAR STRENGTH

APPENDIX A
EFFECT OF THERMAL CYCLING AND CRYOGENIC TEMPERATURES
ON ADHESIVE SHEAR STRENGTH

To determine the effect of thermal cycling and cryogenic temperatures on the shear strength of a particular adhesive, eight samples of carbon bonded to stainless steel were shear tested after thermal cycling between 60°F and -320°F. Two others were shear tested without thermal cycling. The results show that the thermal cycling was not harmful to the adhesive qualities of the epoxy bonding materials tested. Some of the shear tests were performed at room temperature — the others with the specimens submerged in liquid nitrogen at -320°F. The shear strength of the bond was greater at cryogenic temperature than at room temperature.

A.1 BONDED TEST SPECIMENS

Ten specimens were made for the shear tests. Each consisted of AUT83 carbon, approximately 0.125-inch thick, bonded to a 416 Stainless Steel test block, 0.500-inch square by 0.250-inch thick. The bonding surfaces of both the carbon and the stainless steel were ground. The specimens were bonded with Emerson & Cuming's Eccobond 285, using Catalyst 24LV. The adhesive in these specimens was 0.001-inch thick.

A.2 TEST PROCEDURE

Eight of the specimens were thermally cycled between -320°F and 60°F by alternately submerging them in liquid nitrogen and in water. A thermocouple was attached to each specimen to measure its temperature. The transient time from room temperature to -320°F was one minute, and the time from -320°F to 60°F was approximately two minutes. After each down-up cycle, the specimens were inspected.

Four of the specimens were subjected to 13 cycles, and the other four underwent 10 cycles.

The ten specimens were then shear tested, using the test setup diagrammed in Figure A-1. Four were sheared at room temperature, and six were sheared while submerged in liquid nitrogen at -320°F.

A.3 TEST RESULTS

The test results for all ten specimens are shown in Table A-1. The average shear strength of the adhesive bond was:

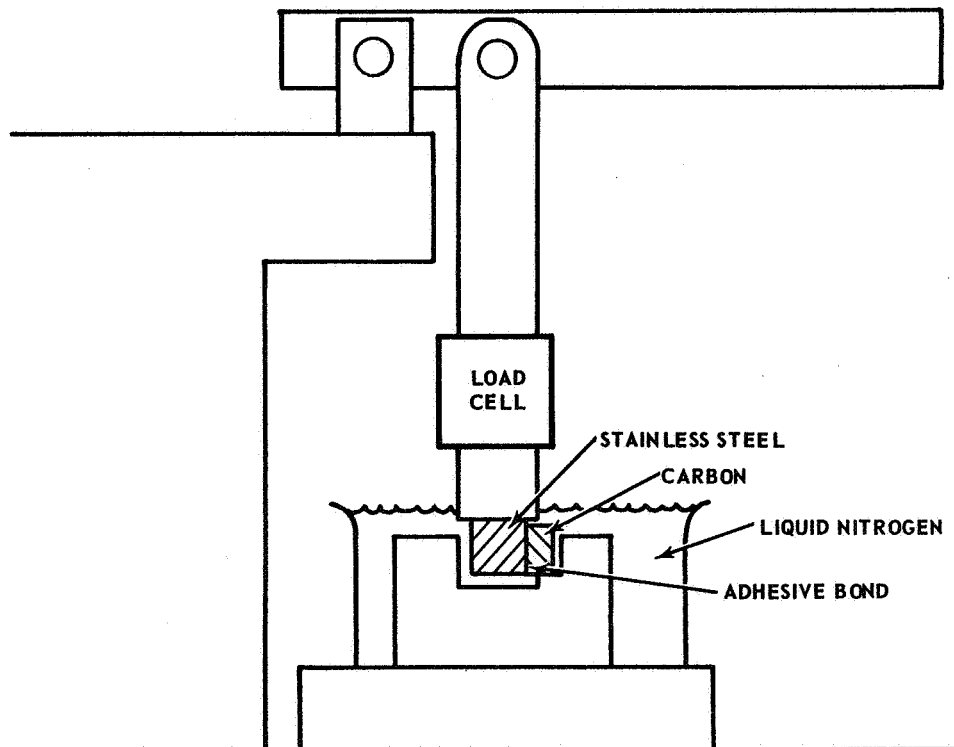
Tests at 70°F - 1065 psi
Test at -320°F - 1550 psi

Table A-1 - Cryogenic Bond Strength

Sample Number	Temperature (°F)	Stress (psi)	Area (sq. in.)	Remarks
1	70	1400	0.216	
2	70	985	0.207	Sample Broke
3	70	776	0.214	Sample Broke
4	70	1105	0.222	Sample Broke
5	-320	1465	0.221	
6	-320	1520	0.221	
7	-320	1148	0.222	
8	-320	1575	0.221	
9	-320	2020	0.214	
10	-320	1580	0.221	

P-4439

NOTE: Samples 1 through 8 were thermal cycled between -320°F and 60°F before shear tests.



P-4439

Figure A-1 - Shear Test Setup

After thermal cycling, the adhesive bond was intact and exhibited good shear strength, although the average shear strength was about 20% below the average of the samples that did not undergo thermal cycling.

All of the specimens had sufficient shear strength, although none exhibited the shear strength predicted in the manufacturer's technical bulletin for Eccobond 285 adhesive. One reason for this apparently is the finish of the bonding surface. These specimens had a ground surface whereas the manufacturer recommends a rough bonding surface.

A.4 DISASSEMBLY OF BONDED PARTS

Since some applications would require disassembly of bonded assemblies, a convenient method of separating the bonded parts is desirable. An effective method was devised for destroying the bond and separating the AUT83 carbon from the 416 Stainless Steel. The samples are heated to 500°F and soaked at this temperature for ten minutes. Then a slight pressure exerted against the carbon removes it cleanly from the stainless steel.

APPENDIX B
DISPLACEMENT AND OUTPUT TORQUE
OF A GEAR MOTOR

APPENDIX B
DISPLACEMENT AND OUTPUT TORQUE
OF A GEAR MOTOR

B.1 NOMENCLATURE

- a - distance from pitch point to final point of contact - in.
- B - pitch point
- C - point of contact
- D - displacement - in^3/rev
- E - center of gear
- F - force resulting from pinion torque
- G - center of pinion
- H - pitch radius of gear plus pitch radius of pinion - in.
- ℓ - gear width - in.
- P_1 - high pressure acting on gears - psig
- P_2 - low pressure acting on gears - psig
- ΔP - difference between P_1 and P_2 - psi
- r_1 - outer radius of gear - in.
- r_2 - outer radius of pinion - in.
- r_{b1} - base radius of gear - in.
- r_{b2} - base radius of pinion - in.
- r_d - radius of tooth profile of gear at point of contact - in.
- r_{df} - radius of tooth profile of gear at final point of contact - in.
- r_i - radius of tooth profile of pinion at point of contact - in.

R_1 - pitch radius of gear - in.
 R_2 - pitch radius of pinion - in.
 T - torque - lb-in
 T_G - torque generated by gear - lb-in
 T_P - torque generated by pinion - lb-in
 T_R - torque transmitted to gear - lb-in
 T_T - torque output of mesh - lb-in
 ϕ - pressure angle - degrees
 ϕ_i - pressure angle at initial point of contact - degrees
 ϕ_f - pressure angle at final point of contact - degrees
 ϕ_m - main pressure angle - degrees
 θ - polar angle - degrees
 θ_i - polar angle at initial point of contact - degrees
 θ_f - polar angle at final point of contact - degrees
 β - initial roll angle - degrees
 $\widehat{\beta}$ - initial roll angle - radians
 α - angular rotation of gear - degrees
 $\widehat{\alpha}$ - angular rotation of gear - radians
 λ - main pressure angle minus pressure angle - degrees

B.2 PRINCIPLE OF OPERATION

Figure B-1 represents one mesh of a gear motor, and P_1 and P_2 are the high and low pressures, respectively, that act upon the gears. To illustrate how a motor functions, the gear and pinion will be looked at separately to see how the pressure difference between P_1 and P_2 act to create an output torque.

The gear is shown in Figure B-2. The arrows shown on the face of the gear teeth represent the pressure in the various tooth spaces acting on the faces of the gear teeth. In tooth spaces 1, 2, and 4, the pressure is equal throughout the space and no unbalanced forces are created; but

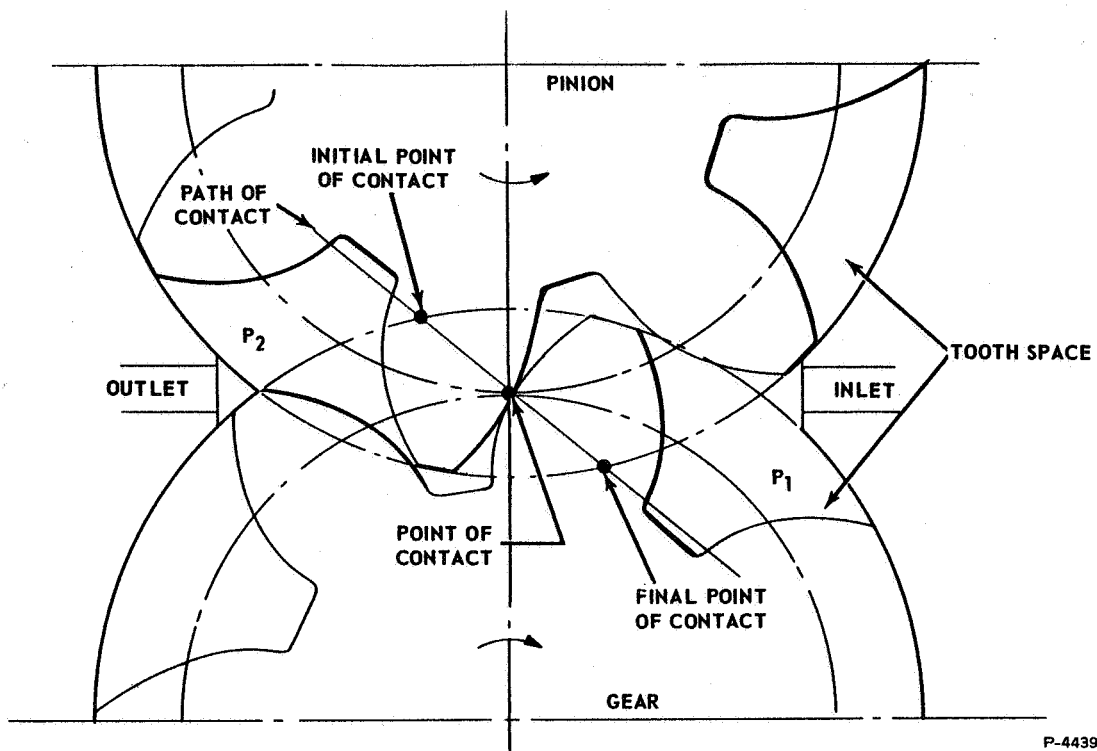


Figure B-1 - Typical Gear Motor Mesh

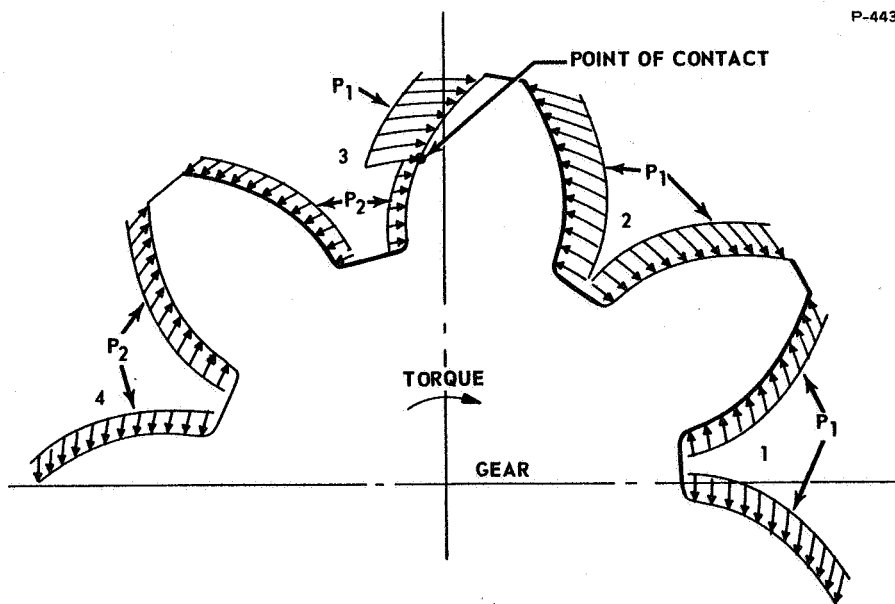


Figure B-2 - Pressure Profile for Gear

in tooth space 3 the high pressure, P_1 , acts along one face up to the point of contact, beyond which the low pressure P_2 acts. P_2 also acts along the opposite face. It can be seen that an unbalance of forces is created that results in a torque in the direction shown.

The high and low pressures act similarly on the pinion, Figure B-3, and the resulting torque is transmitted through the point of contact to the drive gear. The output torque of the mesh is the sum of the torques of the gear and pinion.

The torque generated by each tooth space varies as the point of contact travels along its face. The maximum torque is generated where the point of contact is at its furthestmost point down the tooth, and the minimum or zero torque occurs when the point of contact is at the tip of the tooth. In the meshing of gear teeth, it is the tip of one of the gears that contacts the bottom or the last point of contact of the other so that one gear produces maximum torque while the other is producing zero torque.

B.3 EQUATIONS FOR OUTPUT TORQUE

B.3.1 Output Torque of Gear

To determine the torque output of a gear motor, look at the tooth space of the drive pinion, Figure B-4(a). Between the root of the tooth and the point of contact, the pressure has no effect, but between the point of contact and the tip of the tooth the difference in pressure of P_1 and P_2 (ΔP) acts to produce a torque. The tooth space may be represented as shown in Figure B-4(b), where ΔP is acting on the unit area between r_1 and r_d . The unit area is allowed to rotate about a center E.

Now consider a small area, ℓdr , at a distance r from the center. The torque, dT , developed by this area, will be:

$$dT = \Delta P \ell dr r \quad (1)$$

Summing all the small torques developed between r_d and r_1 :

$$\int dT = \Delta P \ell \int_{r_d}^{r_1} r dr$$

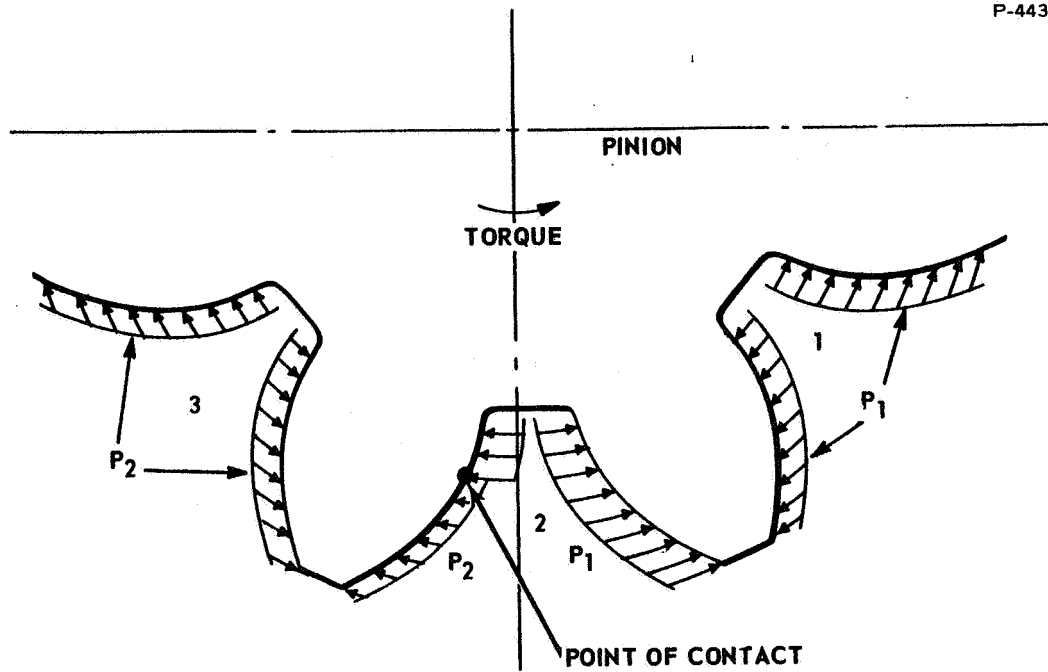
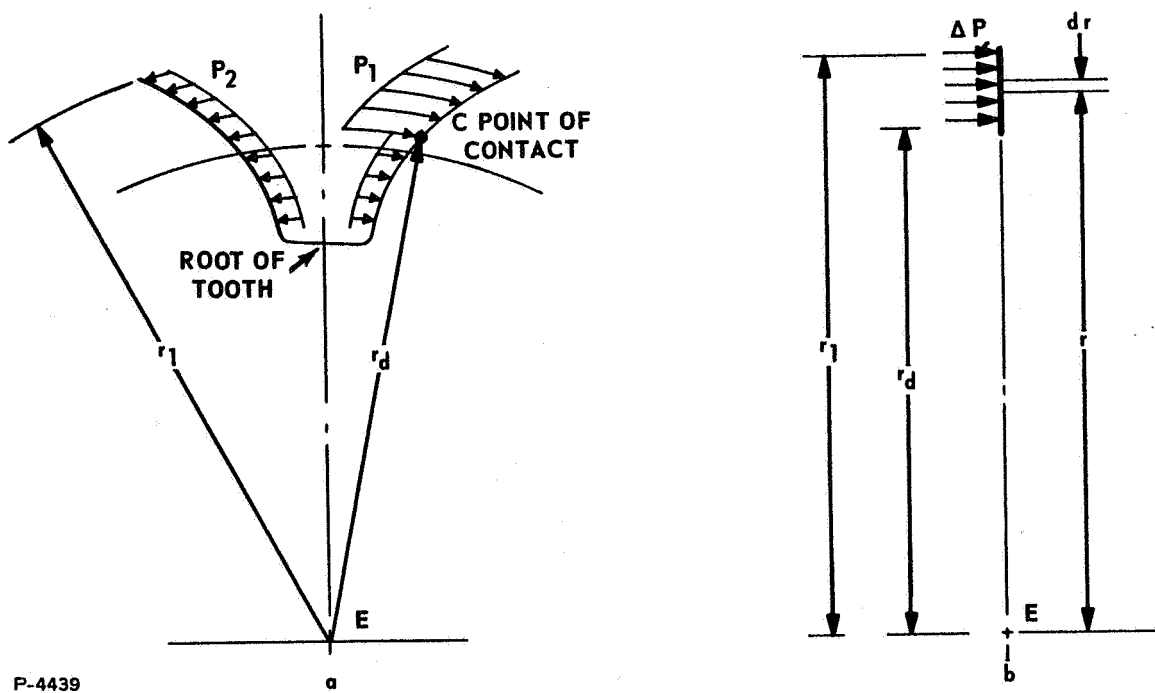


Figure B-3 - Pressure Profile for Pinion



P-4439

Figure B-4 - Diagram for Determining Output Torque

and torque developed by the gear width, ℓ , is:

$$T_G = \frac{\Delta P \ell \left(r_1^2 - r_d^2 \right)}{2} \quad (2)$$

The torque of the pinion may be expressed similarly:

$$T_P = \frac{\Delta P \ell \left(r_2^2 - r_i^2 \right)}{2} \quad (3)$$

where

r_2 = outer radius of the pinion

r_i = radius of tooth profile of the pinion at point of contact.

B.3.2 Total Torque Output

The total torque output of a two-gear motor is the torque output of the gear plus that transmitted from the pinion.

$$T_T = T_G + T_R \quad (4)$$

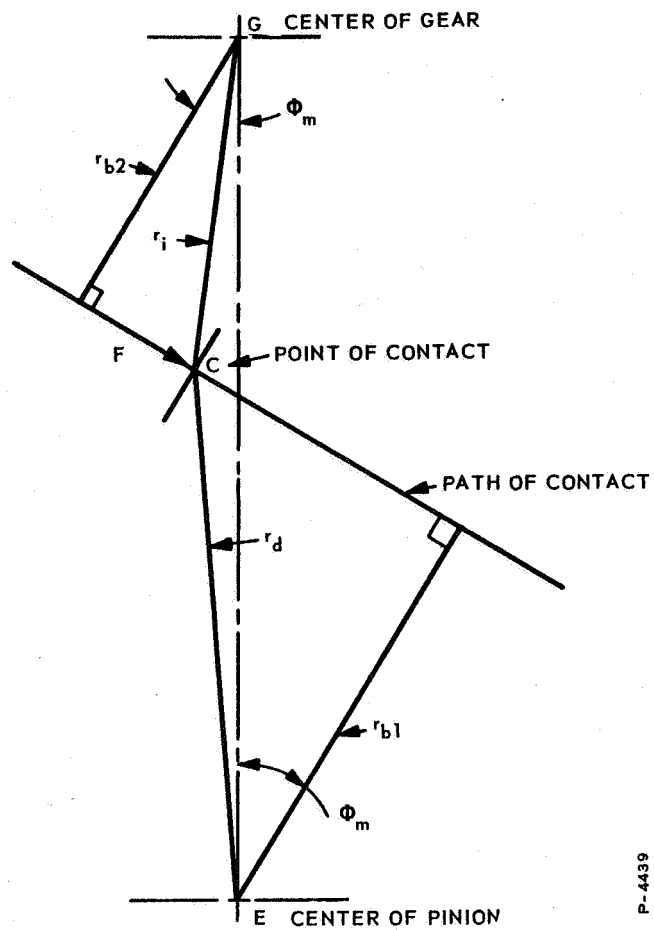
To determine the transmitted torque, look at Figure B-5. The torque of the pinion will result in a force F in the direction of the path of contact acting at the point of contact. This force is equal to:

$$F = \frac{T_P}{r_{b2}} \quad (5)$$

where

T_P = torque of the pinion

r_{b2} = base radius of the pinion.



P-4439

Figure B-5 - Force Diagram in Motor Gear Mesh

The resulting torque in the drive pinion is then

$$T_R = F r_{b1}$$

and

$$F = \frac{T_R}{r_{b1}} \quad (6)$$

where

r_{b1} = base radius of the gear.

Substituting equation (6) into equation (5):

$$\frac{T_R}{r_{b1}} = \frac{T_P}{r_{b2}}$$

or

$$T_R = \frac{T_P r_{b1}}{r_{b2}} \quad (7)$$

The base radii, r_{b1} and r_{b2} , may be expressed as:

$$r_{b1} = R_1 \cos \phi_m \quad (8)$$

$$r_{b2} = R_2 \cos \phi_m \quad (9)$$

thus

$$T_R = \frac{T_P R_1 \cos \phi_m}{R_2 \cos \phi_m}$$

which is reduced to:

$$T_R = \frac{R_1}{R_2} T_P \quad (10)$$

Substituting equations (2), (3), and (10) into equation (4):

$$T_T = \frac{\Delta P \ell \left(r_1^2 - r_d^2 \right)}{2} + \frac{R_1}{R_2} \frac{\Delta P \ell \left(r_2^2 - r_i^2 \right)}{2}$$

which may be written

$$T_T = \frac{\Delta P \ell}{2} \left[\left(r_1^2 - r_d^2 \right) + \frac{R_1}{R_2} \left(r_2^2 - r_i^2 \right) \right] \quad (11)$$

For a given set of gears, r_d and r_i are the only variables in the equation. They may be expressed in the terms of ϕ , ϕ_m , r_b , and the pitch radii R_1 and R_2 . Of these, only ϕ is variable (see Figure B-6).

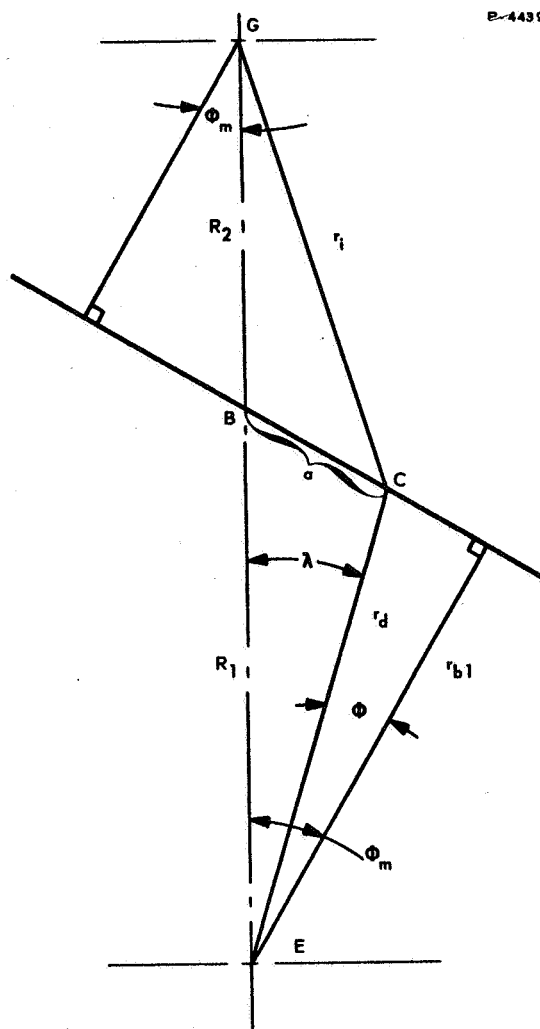


Figure B-6 - Graphical Definition of ϕ , ϕ_m , and λ

$$r_d = r_{b1} \sec \phi \quad (12)$$

$$r_i = (R_1 + R_2)^2 + r_d^2 - 2 (R_1 + R_2) r_d \cos (\phi_m - \phi) \quad (13)$$

By letting $R_1 + R_2 = H$ and $\phi_m - \phi = \lambda$, and substituting equation (12) in equation (13),

$$r_i = H^2 + (r_{b1} \sec \phi)^2 - 2 H r_{b1} \sec \phi \cos \lambda \quad (14)$$

Substituting equations (12) and (14) into equation (11),

$$T_T = \frac{\Delta P \ell}{2} \left\{ \left[r_1^2 - (r_{b1} \sec \phi)^2 \right] + \frac{R_1}{R_2} \left[r_2^2 - H^2 - (r_{b1} \sec \phi)^2 + 2 H r_{b1} \sec \phi \cos \lambda \right] \right\} \quad (15)$$

The equation for torque when the contact point is at the pitch line is:

$$T_T = \frac{\Delta P \ell}{2} \left[r_1^2 - R_1^2 + \frac{R_1}{R_2} \left(r_2^2 - R_2^2 \right) \right] \quad (16)$$

For a three-pinion motor, the torque output would be twice that of the above equation.

$$T = \Delta P \ell \left[r_1^2 - R_1^2 + \frac{R_1}{R_2} \left(r_2^2 - R_2^2 \right) \right] \quad (17)$$

Torque is also equal to:

$$T = \frac{D \Delta P}{2\pi} \quad (18)$$

Combining equations (17) and (18) we have:

$$D = 2 \pi \ell \left[r_1^2 - R_1^2 + \frac{R_1}{R_2} \left(r_2^2 - R_2^2 \right) \right] \quad (19)$$